An Overview of MODIS Capabilities for Ocean Science Observations

Wayne E. Esaias*
Mark R. Abbott, Ian Barton, Otis B. Brown, Janet W. Campbell, Kendall L. Carder,
Dennis K. Clark, Robert L. Evans, Frank E. Hoge, Howard R. Gordon,
William P. Balch, Richard Letelier, Peter J. Minnett

Submitted to Transactions on Geoscience and Remote Sensing
EOS-AM Special Issue
November 4, 1997

*Oceans and Ice Branch, Code 971
Goddard Space Flight Center
Greenbelt, MD 20777
301-286-5465
wayne.esaias@gsfc.nasa.gov

This work was supported by the MODIS Instrument Team Funding from the EOS Project, Mission to Planet Earth.
W. Esaias is with Goddard Space Flight Center, Code 971, Greenbelt MD 20771
Mark Abbott and Richard Letelier are with the School of Oceanography, Oregon State University, Corvallis, OR 97331
Ian Barton is with CSIRO, Australia
O. Brown, R. Evans, and P. Minnett are with the MPO/RSMAS, University of Miami, Miami, FL 33149
J. Campbell is with MTPE/Code YS, NASA Headquarters, Washington, D.C. 20546
K. Carder is with the Department of Oceanography, University of South Florida, St. Petersburg, FL F. Hoge is with the Goddard Space Flight Center, Wallops Flight Facility, Code 975, Wallops Island, VA 23337.
H. Gordon is with the Department of Physics, University of Miami, Coral Gables, FL

ABSTRACT

The Moderate Resolution Imaging Spectroradiometer (MODIS) will add significant new capability for investigating the 70% of the Earth's surface which is covered by oceans, in addition to contributing to the continuation of a decadal scale time series necessary for climate change assessment in the oceans. Sensor capabilities of particular importance for improving the accuracy of ocean products include high signal to noise and high stability for narrower spectral bands, improved on-board radiometric calibration and stability monitoring, and improved science data product algorithms. Spectral bands for resolving solar stimulated chlorophyll fluorescence, and a split window in the 4 micron region for SST will result in important new global ocean science products for biology and physics. MODIS will return full global data at 1 km resolution. The complete suite of Level 2 and 3 ocean products is reviewed, and many areas where MODIS data is expected to make significant new contributions to the enhanced understanding of the oceans' role in understanding climate change are discussed. In providing highly complementary, and consistent set of observations of terrestrial, atmospheric and ocean observations, MODIS data will provide important new information on the interactions between Earth's major components.

INTRODUCTION

Use of satellite image data to investigate oceanic processes has become an essential component of oceanographic research and monitoring. Data from the Coastal Zone Color Scanner (CZCS) provided the first demonstration of the ability to observe the abundance and distribution of phytoplankton chlorophyll in the world's ocean from space [42], [81], [105]. The data has been used extensively to gain better understanding of marine food webs, and the role of the ocean in important biogeochemical cycles including carbon and nitrogen. The near synoptic and global data provided by polar orbiting satellites fill a fundamental need for ocean scientists, since conventional platforms cannot adequately cover the vast, rapidly varying ocean at the appropriate time and space scales [37]. As a result of the importance of synoptic global observations in studying the marine biosphere [81], the U.S. is in the process of implementing three flight missions within four years which will deliver global ocean color data - SeaWiFS (July, 1997), MODIS AM-1 (Summer, 1998), and MODIS PM-1 (December 2000). These missions have been designed to serve the same research community with respect to ocean color, and the overall mission requirements have been highly congruent, while representing an evolution in capability. A primary objective of these missions is to obtain a highly consistent time series of observations useful for understanding the role of the ocean biosphere in the earth system at seasonal to decadal time scales.

Data from the Advanced High Resolution Radiometer (AVHRR), in use operationally since 1981, has provided kilometer-scale estimates of bulk sea surface temperature which are extensively used to study upper ocean dynamics, air-sea fluxes of heat and moisture, and the coupling between biological and physical ocean dynamics.

The MODIS sensors fill both the basic needs established for SST and ocean color, as well as provide advancement in critical capability necessary for decadal time series. Improvements in signal to noise ratio (SNR), band spectral and radiometric performance and characterization, and calibration stability monitoring have been given emphasis [8], [62],

[95]. On the product side, improved spatial and temporal coverage, with addition of new, validated products, are key goals. The purpose of this paper is to highlight the improved capabilities of the current MODIS sensors in relation to the scientific objective and algorithm development, to discuss major product characteristics, and to mention some important areas of post-launch validation and research.

COMPARISONS WITH PRECURSOR SENSORS IN THE VISIBLE

In the visible region, MODIS builds upon the CZCS and SeaWiFS heritage. Two major exceptions to this are that the sensor does not tilt, and the instrument is designed to provide quantitative measurements of solar stimulated fluorescence from chlorophyll *a*. Emphasis has been placed on the ability to monitor sensor calibration and stability through the use of multiple on-board calibrators (including spectral response for the visible and near infrared (VIS-NIR) channels) and by solar and lunar observations, in order to decrease the uncertainty due to instrumental effects in observed trends of geophysical products [38], [61.

The advantage of a tilting sensor is to achieve greater useful global coverage, because the direct specular reflection of the sun can be avoided through tilt changes. However, studies by Gregg [59] and Gregg and Woodward [61] indicate that two nadir instruments collecting data simultaneously, such as planned for EOS AM and PM missions, give approximately equivalent global coverage frequency as a single tilting sensor. Therefore, coverage frequency of the ocean using combined data from the AM and PM sensor should be sufficient to observe the important fluctuations in phytoplankton dynamics.

The ocean color bands on MODIS are very similar to SeaWiFS bands, with the advantage that they are narrower than SeaWiFS, a result of the large aperture and throughput of MODIS. The narrower bands will enhance atmospheric correction. For example the ocean band at 748 nm is about half the width of the equivalent SeaWiFS band, and therefore avoids the nearby atmospheric oxygen absorption feature altogether. Bands 8

and 9 have 15 nm width to achieve needed SNR. MODIS band 11 at 531 nm exhibits the largest band difference from SeaWiFS positions. The analogous SeaWiFS band position is at 510 nm due to the location of the SeaWiFS dichroic beamsplitter [7]. A center wavelength of 531 nm was selected for MODIS to improve the response to accessory pigments, rather than maintain continuity with precursor sensors. Also, there is less spectral structure in this region, and therefore slight on orbit will not significantly affect radiometric calibration.

The positions of the primary ocean bands are given in Figure 1 as bars covering the bandwidth and plotted at the noise-equivalent delta radiance values (NEDL) for each band. Exact band shapes are illustrated in Barnes et al. [8]. Also shown on this figure are modeled top of the atmosphere and bottom of the atmosphere (just above the ocean surface) signals over the ocean for extremely low and extremely high chlorophyll concentration. Note that the two lines for top of the atmosphere values are virtually congruent, indicative of the very small radiance differences which must be detected by the sensor. Modeled radiance values show nearly the full dynamic range of oceanic chlorophyll concentration of interest. The position of MODIS high resolution bands which might also prove useful for ocean color observations are also indicated.

The signal to noise ratio (SNR) is one of the key scientific requirements and is carefully specified for ocean color sensors, due to the fact that the oceans are quite dark. Water-leaving radiance values are commonly less than 10 percent of the total radiance measured at the sensor, and often are less than a percent. The scientific requirements for various sensors have increased from CZCS to MODIS, based on demonstrated need for higher precision and accuracy at very low chlorophyll levels to address vast open ocean provinces, and to accommodate improvements in atmospheric and bio-optical algorithms. The principles used to determine required SNR for SeaWiFS and MODIS are comparable, and differ primarily only in the amount of total error allocated to the sensor compared to the error in the atmospheric correction and in-water algorithms for chlorophyll. All contribute to the total error in derived chlorophyll pigment concentration which

is compared to CZCS experience. This has been discussed in some detail by Gordon and Wang [57]. Briefly, the specified SNR for the SeaWiFS sensor were based on equalizing error contributions in derived chlorophyll concentrations from a) the sensor and b) the CZCS algorithms. The MODIS SNR specifications are more stringent in order to reduce sensor-induced errors when applying much improved geophysical algorithms developed for SeaWiFS and MODIS.

Large differences in the radiance value at which required SNR was specified exist between various sensors. Because SNR is an instrument specific, non-linear function of input radiance, direct comparison of minimum SNR specification values for various instruments without reference to the input radiance at which it is measured can be misleading. Table 1 shows the ocean band center wavelengths, specified SNR, and the input radiance (L_{in}) at which the SNR is required for the three ocean color sensors. Included are specifications for four higher resolution bands (500 meter bands 3 and 4 at 470 and 555 nm and the 250 meter bands 1 and 2 at 670 and 865 nm, respectively). Different L_{in} values were used in specifications because different radiative transfer and algorithm models and viewing geometries were used in analyses. Pixels near the edge of the swath (which are brighter than at nadir) with a 20 degree solar zenith were chosen as the arbitrary reference for SeaWiFS specifications, resulting in specifying SNR at relatively high L_{in} values, while pixels near nadir at a lower sun angle were used in model studies for MODIS.

For comparison, the specified SNR for various sensors have been computed for a common set of input radiance values given by the modeled spectra for top of the atmosphere radiance as a standard. Table 1 provides the adjusted SNR and the model values (which are those plotted in Figure 1 for high chlorophyll). The model uses an exact Rayleigh calculation with single aerosol scattering. The aerosol optical depth at 670 nm was 0.2, with an Angstrom exponent of 0.5, and 0.5 cm water and 0.35 cm ozone in the air column. The view is nadir with a solar zenith angle of 60 degrees, and chlorophyll concentration was 10 mg m^{-3}.

Performance of the CZCS at the model radiance levels was determined using preflight calibration and performance data plots provided by the manufacturer, Ball Aerospace Systems

Division. Performance of SeaWiFS at model radiance values were interpolated from Table 26 in the SeaWiFS Prelaunch Sensor Acceptance Report [7], again based on measured performance test data. Values for SeaWiFS in column 4 of Table 1 are taken from Table 14 of Barnes, Holmes et. al. [8].

For MODIS, there remain slight differences between specified L_{in} and the model values (which arise again because of slight differences in viewing geometry and atmospheric conditions between this model and the analysis actually used to set the SNR requirements). SNRs expected at model radiance values were estimated by using the relationship:

$$\mathbf{SNR}_{mod} = \mathbf{SNR}_{spec}(\mathbf{L}_{mod} / \mathbf{L}_{spec})^{0.6} \quad (1)$$

where the subscripts refer to *mod*el value or *spec*ification value.

The adjusted SNR_{model} values given in Table 1 are plotted as a function of wavelength in Figure 2, demonstrating improvement in SNR through the CZCS-SeaWiFS-MODIS progression, each increasing roughly by a factor of 2. The requirement for very high SNR to quantify solar induced chlorophyll a fluorescence is apparent in the two MODIS bands near 670. The figure illustrates that several of the MODIS high resolution bands slightly exceed CZCS performance at their higher resolution. This could prove useful in coastal and estuarine regions where higher spatial resolution can be used to avoid contamination by shorelines, and to resolve generally smaller hydrodynamic turbulence scales than are found in the open ocean, although at-launch algorithms do not incorporate these bands. The equivalent SNR for these bands will increase as data are spatially averaged, and they will not saturate when viewing bright targets.

PRODUCT DESCRIPTIONS

The Level 2 ocean color products which will be derived from MODIS at launch are given in Table 2. The algorithms which have been developed by science team members are described in Algorithm Theoretical Basis Documents (ATBDs) which are available through the EOS Project Science Office electronically at

http://eospso.gsfc.nasa.gov/eospso_homepage.html. Summaries are also available in the EOS Data Products Handbook at the same location Included here are brief synopses which emphasize the expected improvements with MODIS.

The data products will be available at Level 2 in 1000 km along track granules, and in several earth gridded temporal and spatial resolutions. For Level 3, the standard gridded product is an equal area sinusoidal grid, similar to the SeaWiFS grid, but at 4.2 km spatial resolution. Standard mapped products at lower resolution are also enabled in software. A series of 1 degree resolution products is also envisioned.

For ease of discussion, the data products are produced in five basic groups - atmospherically corrected ocean reflectance group, a semi-analytic bio-optical group, an empirical bio-optical algorithm group together with fluorescence and phycoerythrin, sea surface temperature, and ocean productivity (a Level 4 product in a sense, because the inputs are Level 3 products). Table 2 shows these groups, and cross-references to the EOS Data Products Handbook and ATBD designations. The relationship of the Level 2 ocean color products are shown in figure 3 and are discussed briefly here.

Atmospheric Correction

The portion of the radiance reflected from the ocean atmosphere system that was backscattered *out* of the water, and thus contains information about oceanic constituents, is at most 10% [55]. This maximal return occurs in the blue at very low concentrations of chlorophyll *a*. In the green, or for larger values of chlorophyll *a* in the blue, the ocean-penetrating fraction is considerably smaller. The rest of the reflected radiance seen by the sensor is scattered from the atmosphere and the sea surface. Retrieval of the relevant oceanic signal from the total radiance is termed atmospheric correction.

Atmospheric correction algorithms were developed for the CZCS by Gordon and coworkers [45], [50-53]. These were crude in the sense that multiple scattering in the atmosphere was ignored; however, sensors like MODIS are significantly better than CZCS

in radiometric performance, and to take full advantage of the improved radiometry, more precise atmospheric correction is required. Algorithms that achieve the required accuracy have been developed for SeaWiFS and MODIS, and a comprehensive review of the present state of atmospheric correction is provided in Gordon [47]. We provide a brief description of the MODIS atmospheric correction algorithm next.

As it is now possible to calibrate sensors directly with respect to the sun, it is preferable to use the generalized reflectance rather than the radiance. The reflectance ρ is related to the radiance L through $\rho = \pi L / F_0 \cos\theta_0$, where F_0 is the extraterrestrial solar irradiance, and θ_0 is the solar zenith angle. The top-of-atmosphere (TOA) reflectance ρ_t is given by

$$\rho_t = \rho_r + \rho_a + \rho_{ra} + t\rho_w + t\rho_{wc} + T\rho_g, \qquad (2)$$

where the subscripts *r*, *a*, *ra*, *w*, *wc*, and *g*, refer, respectively, to the contribution to the reflectance from Rayleigh scattering in the absence of aerosols, the contribution of aerosol scattering in the absence of air molecules, the contribution from interactions involving both molecular and aerosol scattering, the contribution from photons backscattered *out* of the water (the desired *water-leaving reflectance*), the contribution from whitecaps on the sea surface, and the contribution from photons specularly reflected from the sea surface without ever interacting with the atmosphere (sun glint). In this equation, *t* is the diffuse transmittance of the atmosphere, and *T* is the direct transmittance. The contribution from sun glint can be very large near the specular image of the sun (where the sensor would be viewing the image of the sun reflected from a *flat* sea surface), but falls rapidly away from this point. The water leaving signal in this region cannot be retrieved accurately, and the data there must be discarded. Thus, we ignore the contribution of ρ_g, by virtue of discarding the imagery where it is significant. The zone for which data cannot be processed is delineated by an estimate of the wind speed (from numerical weather assimilation models) along with the Cox and Munk [34] model of the sea surface [47]. The whitecap contribution is small and can also be

estimated from an estimate of the wind speed [44], [56]. The Rayleigh scattering contribution can be precisely computed given the surface atmospheric pressure [48], which is also estimated from numerical weather models. Derivation of ρ_w from ρ_t still requires estimating $\rho_A \equiv \rho_a + \rho_{ra}$. This is the most difficult aspect of the atmospheric correction problem, because at the Level of accuracy required for modern sensors, multiple scattering affects cannot be neglected. It is even more complex because simulations [45], [47] show that the influence of multiple scattering is dependent on the physical-chemical properties of the aerosol, as well as on its concentration. Thus, in order to evaluate the amount of multiple scattering a model for the aerosol properties must be assumed or determined from ρ_t. Fortunately in Case 1 waters, i.e., waters for which phytoplankton and their immediate decay products control the optical properties of the water [55], $\rho_w \approx 0$ in the near infrared (NIR). MODIS has two spectral bands in the NIR that possess this property: 748 nm and 869 nm (Bands 15 and 16). Thus, for these bands it is possible to estimate ρ_A at each pixel in Case 1 waters. The spectral variation of ρ_A between these two wavelengths can then be used to select an aerosol model (actually two) from a list of possible candidates. Presently, the candidate aerosol models that are used in the MODIS atmospheric correction algorithm are those provided by Shettle and Fenn [100]. The chosen candidate aerosol models are then used to extrapolate ρ_A into the visible. This extrapolation is effected through a set of lookup tables (LUTs) that provide ρ_A as a function of the aerosol concentration for all sun-viewing geometry's. The LUTs are computed for each candidate aerosol model using a two-layer radiative transfer code with all of the aerosol scattering in the lower layer and the Rayleigh scattering in the upper layer.

The atmospheric correction algorithm described above has been shown to be capable of retrieving the water-leaving reflectance with the required accuracy under most oceanic conditions. However, problems are encountered when the aerosol is strongly absorbing, e.g., urban pollution or desert dust transported over the oceans by the winds. The difficulty with absorbing aerosols is two fold [47]. First, the spectral variation of ρ_A in the NIR is for the most part determined by the size distribution of the aerosol and is very weakly

dependent on its composition therefore weakly- and strongly-absorbing aerosols with similar size distributions cannot be differentiated. Second, in contrast to weakly-absorbing aerosols, the influence of strongly-absorbing aerosols on ρ_A shows a significant dependence on their vertical distribution. Recently, Gordon et al. [54] have proposed an algorithm that shows considerable promise in dealing with both weakly- and strongly-absorbing aerosols in Case 1 waters. The basic idea is that, because the effects of strong absorption on ρ_A are manifest in the blue portion of the spectrum, where there is significant multiple scattering due to the large Rayleigh optical thickness even at small aerosol concentrations, it is necessary to do atmospheric correction and retrieve the bio-optical parameters simultaneously. Briefly, $\rho_A(\lambda)$ is computed for each candidate atmospheric model as a function of aerosol concentration. Similarly, $\rho_w(\lambda)$ is computed as a function of the ocean's constituent concentrations (chlorophyll *a*) using a bio-optical model [48]. All of the parameters (aerosol model and concentration, and ocean constituent concentrations) are then systematically varied until the differences between the observed and modeled $\rho_A(\lambda) + t(\lambda)\rho_w(\lambda)$ reach a minimum in an RMS sense. This minimum provides the desired atmospheric and oceanic parameters. This algorithm is presently undergoing extensive testing. It can be expected to run much slower than the at-launch version; however, the strategy will be to utilize it at reduced resolution for the purpose of assessing the probability of having absorbing aerosols and finding an appropriate set of aerosol models.

Empirical Algorithms

Phytoplankton biomass is usually expressed in terms of chlorophyll *a* concentration because of the ease of making these measurements, and because all photoautotrophs contain chlorophyll a in the primary reaction centers. It remains the primary derived product used by biological oceanographers. The empirical algorithms are based on relationships between in-situ optical measurements of remote sensing reflectance or normalized water leaving radiance (nL_W), and simultaneous property concentration measurements. To account for optical signal attenuation, the in-situ concentrations are weighted according to the diffuse attenuation coefficient [50]. These relationships are then applied using satellite derived nLw, and compared with simultaneous chlorophyll data collected at the time of satellite overpass. In situ measurements are made according to established protocols [89].

Initial CZCS results reported by Gordon et al. [51], demonstrated an excellent potential for achieving the CZCS goal of measuring phytoplankton pigment concentrations to within about a factor of 2. The pigment retrievals, when compared to the shipboard measurements, yielded an agreement to better than 0.5 in $\log_{10}$ C, where C is the sum of the chlorophyll a and phaeopigment a pigments in mg m^{-3} . In general, within their comparison there appears to be a trend towards under estimating the pigment concentration with the CZCS algorithms. A source for this under estimation lies within the preliminary pigment algorithm itself. This bias was corrected by recasting the preliminary pigment algorithms with the addition of data from post-launch validation cruises into forms which are specific to this remote sensing application and the CZCS spectral characteristics. The purpose of implementing these modifications was two-fold: to reduce the sources for systematic bias in estimating the pigment concentrations, and to provide a computation which incorporates the depth dependence of the optical signal and the variations in the vertical distribution of phytoplankton. Phytoplankton pigment algorithms, for example, require an accurate determination of water leaving spectral radiance. Actually, only the spectral character needs

to be retrieved accurately, since within this algorithm scheme only radiance ratios at different wavelengths are used, resulting in some reduction of errors.

The basic form which satisfies the MODIS bio-optical at-launch empirical products is:

$$\log \text{Product} = A(\log X)^3 + B(\log X)^2 + C(\log X) + D/E, \quad (3)$$

where, A,B,C,D and E are least-squares regression coefficients or constants, and

$$X = \frac{(e)nLw(band9,443) + (f)nLw(band10,490) + (g)nLw(band11,531)}{nLw(band12,550)} \quad (4)$$

Here the constants e, f, and g are 0 or 1 and are used to select the spectral bands employed to derive the specific product. The preliminary coefficients (Table 3) are based on the original CZCS experimental database adjusted for the SeaWiFS bandwidths. These coefficients will be revised prior to launch for the MODIS spectral band characteristics and use of the new in-situ bio-optical database. This form accommodates up to four principle wavelength bands which are employed in the empirical derivation of bio-optical products in either single or multiple wavelength ratios. It will be used to generate the following at-launch products for Case 1 waters: CZCS Pigments (chlorophyll a plus phaeopigments), chlorophyll a (Case 1), Diffuse Attenuation Coefficient (k 490 nm), and suspended solids.

Recent comparisons by O'Reilly and Maritorena [92] between pairs of in-situ optical and pigment concentration resulted in a third order polynomial relating chlorophyll *a* and the ratio of SeaWiFS bands 3 and 5 with very small apparent error or bias. This relationship is presently used for SeaWiFS, and can be easily accommodated using MODIS bands 11 and 12 in equations 3 and 4. It will be considered for MODIS following validation of SeaWiFS data products.

Coccoliths and Calcite

Coccoliths are small calcite ($CaCO_3$) plates produced by a distinct taxon of marine phytoplankton, the coccolithophores, which are cosmopolitan in the oceans. Several species, notably *Emiliana huxleyi*, form dense blooms in temperate and subarctic waters [18] which are highly visible due to increased optical scatter from the coccoliths. Coccoliths are continually produced on the surface of the flagellated algal cell, and become detached with time. During the latter phases of blooms the free coccoliths greatly exceed those attached. The coccoliths serve as very efficient, white, optical scatterers. Because of the anomalous light absorption to scattering ratio in these blooms, basic assumptions for atmospheric and bio-optical algorithms are violated and the chlorophyll a retrievals can be heavily impacted [49]. These organisms play a unique role in the ocean carbon biogeochemical cycle, since large amounts of calcite are exported to the deep ocean during such blooms [67]. Additionally, this species is a primary source of oceanic dimethyl sulfide, with implications on cloud formation and coverage [25]. They also provide opportunity to study the population dynamics of a single plant species with remote sensing, which is rare in both the terrestrial and marine biospheres. For these reasons it is important to correct the chlorophyll algorithms for their presence, as well as to derive their abundance and calcite concentration.

The MODIS coccolith products are derived using a semi-analytic approach in conjunction with of the atmospheric correction process. Look-up tables relating anomalous spectral scattering to the coccolith concentration, and to the calcite concentration, are used to retrieve a more accurate chlorophyll product within the blooms as well. This approach differs from the SeaWiFS at-launch coccolith algorithm [17] which is used to classify blooms and to compute their area but which does provide concentration values. The MODIS algorithm will undergo extensive testing using both SeaWiFS data and with a substantial collection of *in situ* optical backscatter, calcite, and coccolith determinations made over the past several years in the Atlantic [5-6] and Indian Oceans. An extensive ship-board algorithm validation effort is already underway using SeaWiFS observations. For

MODIS, it is expected that several of the ocean bands may show saturation at high coccolith concentrations, where surface reflectance can exceed 25%. Under those conditions the use of MODIS bands 1 through 4 can be substituted.

Semi-analytic Bio-Optical Algorithms

The semi-analytical, bio-optical model of remote-sensing reflectance (e.g. normalized water-leaving radiance) developed by Lee et al. [75] provides the basis for the MODIS algorithm for the concentration of chlorophyll *a* as well as for calculations of absorbed radiation by phytoplankton (ARP). The latter quantity is utilized by the MODIS chlorophyll fluorescence algorithm (see below) to form a parameter indicative of the physiological state of phytoplankton, the quantum yield of fluorescence.

The algorithm is developed such that four quantities are determined: chl *a*, absorption by gelbstoff (dissolved blue absorbing organic matter) at 400nm, absorption coefficient of phytoplankton (expressed at 675nm), and ARP. With these variables, the total absorption coefficients for the visible region can be deduced through use of algorithm parameters. ARP also depends upon the instantaneous flux of photons per wavelength interval just beneath the sea surface [60] which is calculated as part of the instantaneous photosynthetically available radiation algorithm (IPAR) [23]. ARP is an expression of the quanta absorbed by phytoplankton in the top 3m of the water column, the interval from which more than 90% of the upwelling fluorescence photons which are seen by the sensor originate.

A unique aspect of the MODIS chlorophyll *a* algorithm is that it is not based on a simple regression equation using the global database. It is instead physically-based for the optical portions of the algorithm, and empirically based for the bio-optical portions. The bio-optical parameters, however, change with the dominant species assemblage on a seasonal and geographic basis, driven by changes in nutrient and light availability and temperature, and various bio-optical domains are deduced empirically using MODIS sea-

surface temperature data as compared to the Kamykowski [71] nitrogen-depletion temperatures for a given location [22]. This relationship between nutrients and temperature results from the deep-mixing or upwelling of cool, nutrient-rich waters found beneath the surface mixed layer as reflected in the historic nutrient-temperature data base of the National Oceanographic Data Center of NOAA.

Identification of bio-optical domains improves chlorophyll *a* retrievals from about $\pm$ 50% uncertainty to less than $\pm$ 30% uncertainty (see Fig. 4). Also, since the spectral absorption coefficient of seawater can be determined by summing the absorption components of gelbstoff, phytoplankton, and water, it is possible with MODIS data to calculate the depth of penetration of light into the upper ocean and the resulting vertical distribution of heat due to insolation.

Clear-Water Epsilons

Since atmospheric radiance can be 10 times that of water-leaving radiance, aerosol radiance must be accurately deduced in order for ocean-color algorithms for chlorophyll *a* to be at all accurate. Estimates of the aerosol radiance received by MODIS over the ocean depend upon spectral extrapolation of the behavior of aerosol backscattering based upon measurements in the infrared where the ocean is "black". Marine aerosols are largely nonabsorptive and predominate over the ocean most of the time. Occasionally, red iron-rich dust from the Sahara and Gobi deserts, for example, are carried across the north Atlantic and Pacific basins, and they absorb significantly at blue wavelengths, as do phytoplankton.

The clear-water epsilon algorithm is designed to flag blue-absorbing aerosols based upon our "*a priori*" knowledge of the water-leaving radiance at 532, 551 and 667 nm which are stable for waters with chlorophyll *a* values less than about 0.4 mg/m^3 (hence "clear water"). The epsilon values are based upon spectral ratios of aerosol reflectance values (e.g. $\rho_a(531)/\rho_a(667)$) [53].

Flagging for data points with epsilon values less than about 0.95 provides an indication of absorption at the blue end of the spectrum and is indicative of iron-rich aerosols. These flagged pixels must be corrected with a nonstandard algorithm during a reprocessing phase. Iron can be a limiting nutrient in the open ocean. A research objective is to spectrally quantify the fraction of iron present in terrigenous aerosols.

Phycoerythrin

There are 3 major algal pigment groups found in marine phytoplankton and bacteria: the chlorophylls, carotenoids, and phycobilins [13]. The major phycobilins are phycoerythrin (PE) and phycocyanin. The phycoerythrins are a class of pigment-protein macromolecules with chromophores that absorb light in the ~480-580 spectral region. These chromophores are of two types: phycoerythrobilin (PEB) which absorbs in the 565 nm region and phycourobilin (PUB) which absorbs in the 495 nm region. PEB is a component of the photosynthetic light harvesting system and is found in all PE-containing marine cyanobacteria. The PE spectral absorption band peaks near 565 nm when only PEB chromophores are present and 10- 15 nm lower when PUB chromophores are present.

PEB has been observed by active (laser) airborne fluorescence methods since 1979 [63] and recognized in upwelled radiance values since 1986 [64-65]. Phycoerythrin fluorescence was detected as an increase in the 560-600 nm region of surface upwelling irradiance spectra in Lake Washington [32].

The PEB concentration is derived as a research product by numerical radiance model inversion of nL_w. Previous oceanic radiance model inversion theory described retrieval of three inherent optical properties (IOP's): total backscatter, absorption coefficient of chromophoric dissolved organic matter (CDOM) and the absorption coefficient of phytoplankton [66]. The radiance model inversion theory has been extended to accommodate absorption at ~565 nm due only to PEB pigment, absorption of PEB at ~545 nm (when PUB substitution occurs at some selected PE chromophore sites), and PUB

absorption at ~495 nm. The PEB absorption coefficient retrieval will be validated by comparison with airborne laser-induced PEB fluorescence and with published laboratory values of PEB absorption coefficients.

Phycoerythrin retrieval is an important research product which will enable scientific investigation of the global distribution of the phycoerythrin pigment and the diversity of phycoerythrin-bearing species, especially cyanobacteria. The PE-containing organism *Trichodesmium* is the major ocean nitrogen fixer. Since fixed nitrogen commonly limits phytoplankton production in the ocean, oceanic nitrogen fixation has direct links to the ocean carbon cycle [72], [41]. At times, oceanic carbon production by cyanobacteria is greater than that the larger phytoplankton.

Ocean Primary Production

For ocean applications, primary productivity is the net rate of carbon fixation by phytoplankton through the process of photosynthesis, as measured by the radiocarbon uptake technique using water samples incubated either at the depth from which they were collected, or in simulation incubators. Units of production are gm Carbon m^{-2} day^{-1}. Rates estimated for weekly and annual time periods simply equal the summation of the daily rates, or integration using trapezoidal interpolation. Ocean primary production rates reflect the fact that phytoplankton biomass, as estimated by chlorophyll concentration, can experience up to several doublings per day.

Of interest to global biogeochemical cycle studies is the amount of organic carbon which sinks from the sunlit zone through the upper mixed layer to enter the deep ocean, where the CO_2 resulting from its decomposition is removed from direct contact with the atmosphere for extended periods. This portion of net production is called export production. Primary production can also be differentiated according to whether the phytoplankton use nitrogen which originates from recycling within the upper mixed layer grazing population (recycled production), or conversely, whether the nitrogen is "new" to the mixed layer as a result of upwelling or seasonal mixing (new production). New

production is typically reported in nitrogen units because it is approximated by the uptake of nitrogen in the form of nitrate which results from fully oxidized organic matter [34].

The major variable determining marine primary production for any given day is the biomass of phytoplankton, which itself results from previous production. Light spectral intensity as a function of depth, nutrient availability, temperature, and other factors, such as intensity of mixing, advection, and zooplankton grazing are also quite important.

The MODIS Primary Production product provides two estimates, or indexes, of short term net carbon production, and separate estimates, on annual scales, of net carbon production, export carbon production, and new nitrogen production, using empirical annual algorithms.

The two short term index calculations are performed using weekly (8-day) averaged chlorophyll. concentration, and produce estimates of total carbon production for the global ocean region. The first index, developed by Behrenfeld and Falkowski [12] estimates daily production in the euphotic zone as a function of surface chlorophyll *a*, daily integrated photosynthetically available radiation (PAR), day length, and the maximal rate of carbon production per unit chlorophyll a as a function of depth within the euphotic zone ($P_{b,\ opt)}$. When $P_{b,opt}$ is plotted against temperature for a wide range of global and seasonal in-situ data, a strong relationship is apparent. Therefore, its local value is parameterized as function of SST. The euphotic zone is the depth interval from the surface over which 99% of sunlight is attenuated, and is calculated from MODIS products.

The second short term index, developed by Howard and Yoder [68], uses a similar approach, but requires an independent estimate of the physical upper mixed layer depth, rather than the euphotic depth, for integration. The mixed layer depth as determined by the Navy's OTIS numerical ocean assimilation model is used for this variable. A second difference is that the maximum rate of production per unit chlorophyll a as a function of light intensity (P_{max}) is used as the light utilization efficiency factor instead of $P_{b,\ opt}$. P_{max} is parameterized as function of SST, different from that used for $P_{b,\ opt}$. The short

wave incident radiation field available from the Data Assimilation Office at Goddard is used to estimate daily integrated incident PAR for both products.

The two approaches produce different distributions on short time scales, but which appear to converge (to within 30%) when integrated globally over the year [12], [67-68], and with other estimates based on models [96] and satellite data as discussed in [41], [79], [96]. Development of a consensus algorithm is the focus of NASA's Primary Productivity Working Group NPPWG [41]. It is expected that intensive applications using SeaWiFS data and early MODIS data will improve convergence, and will be useful in assessing the overall uncertainty and errors between these and other, different approaches within various oceanographic regimes. The approach described here for the evolution of this product is in keeping with the science strategy issued by the NPPWG [41].

The annual primary production estimate is based on simple linear relationships between annual production terms and chlorophyll a averaged over a year developed by Iverson, et al. [69]. These relationships hold for those portions of the open ocean which show high annual variance in Level-3 chlorophyll concentration (HV regions). Annual carbon production, export production, and new production are computed at weekly intervals using a running annual (46-eight day week) average. The linear relationships explains 98% of the variance in the production-chlorophyll plots for the high variance areas. These areas occupy about 28% of the global ocean based on the CZCS analysis. The HV areas account for about 70% of the global Export Production and New Production components, but only about 30% of Total carbon Production [69]. On annual scales, there is no simple linear relation between average chlorophyll and production terms in the low annual chlorophyll variance portion of the ocean.

Solar Stimulated Chlorophyll Fluorescence

Light energy absorbed by phytoplankton chlorophyll has one of three fates. Most (more than 90%) is lost at heat. Some (up to 12% can be converted to chemical energy via the process of photosynthesis. Another small and variable fraction (up to 3%) is re-emitted

as fluorescence. Solar stimulated chlorophyll fluorescence appears as a distinct peak centered at 683 nm in the upwelling radiance spectrum in natural waters (Figure 1). This peak produces a positive deviation from the expected sea surface leaving radiance of pure water and has been studied by numerous researchers using in situ as well as remote sensing devices mounted in aircraft [43], [46], [58], [74], [91].

As a result of studies of sun stimulated fluorescence, satellite sensors capable of measuring chlorophyll fluorescence from low earth orbits are being developed, the first of which is MODIS. Using narrow bands centered at 665.1, 676.7, and 746.3 nm (Figure 5), this sensor will be able to detect chlorophyll fluorescence signals at 676.7 nm (Fluorescence Line Height, or FLH) as low as 0.012 Wm^{-2} sr^{-1} μm^{-1} [76].

By dividing the FLH by the rate of energy absorbed by the photosynthetic systems (Absorbed Radiation by Phytoplankton; MODIS-21 product) it will be possible to estimate a Chlorophyll Fluorescence Efficiency (CFE) which is proportional to the fluorescence quantum efficiency.

Relationships between fluorescence efficiency and productivity

In recent years research has been focused in the use of sun stimulated fluorescence to estimate photosynthetic rates [73], [26]-[27]. Based on Butler's tri-partite model of the photochemical apparatus [19] we should expect to observe that the quantum efficiency of fluorescence varies inversely to the quantum efficiency of photosynthesis because both processes are competing for energy during the de-excitation of chlorophyll. However, the relation is not simple and may not work over a wide range of oceanic conditions considering that the de-excitation of chlorophyll resulting in heat dissipation is the major dissipation pathway [40].

Semi-empirical algorithms used to estimate primary productivity (PP) from remote sensing platforms are based on our the ability to monitor remotely available irradiance (E) and chlorophyll concentration [chl] in the surface of the ocean. However, in order to obtain an accurate estimate of photosynthetic rates we also need to know the amount of available

energy being absorbed by the photosystem (the product of E, [chl], and the specific absorption coefficient a*) and the fraction of absorbed energy being stored in organic matter. This fraction is also known as the photosynthetic quantum efficiency (Φp). Neglecting spectral effects for illustrative purposes, on a unit volume basis, this is indicated by:

$$PP = E\ [chl]\ a^*\ \Phi p \quad (5)$$

The remote sensing estimation of chlorophyll concentration in surface waters is derived from the reflectance or upwelling radiance ratio between wavelengths within the main absorption band of phytoplankton pigments and wavelengths outside this band [28]. Consequently, this estimation is derived from the rate of light absorption by algae and corresponds to the product of E, [chl], and a* [77]. In the case of fluorescence, a similar simple equation for fluorescence emission, again ignoring spectral effects for the sake of simplicity, is:

$$F = E\ [chl]\ a^*\ \Phi f \quad (6)$$

where Φf is the quantum efficiency for fluorescence.

Although developing relationships between Φf, CFE and photosynthetic quantum efficiency (Φp) will not be straightforward, recent in situ studies suggest that variations in CFE may prove useful as indicators of changes in the nutritional status of phytoplankton [77]. Furthermore, spatial and temporal studies addressing the variability of CFE may also help us to better understand and predict the variability in Φp [1]. Knowledge of the scales of variability of Φp will allow a better estimation of some of the errors associated with the calculation of primary productivity using semi-empirical algorithms, especially the errors associated with variations in Pmax or Pb,opt, and a*.

Sea Surface Temperature

Precursor Instruments in the Infrared Region

MODIS builds on the experience of the NOAA Advanced Very High Resolution Radiometer (AVHRR) [96]-[97] and the ERS Along Track Scanning Radiometer (ATSR) [35], [85]-[87] missions. Bands used in SST determination for MODIS and other missions of interest are shown in Table 4. These particular bands were chosen for MODIS based on specific aspects of the atmospheric total column transmissivity in each part of the mid- and far-infrared spectrum. Figure 8 presents a profile of the expected earth radiance at satellite height from 3 μm to 14 μm. AVHRR experience suggested improvement of blackbody design and lowering of NEDTs for the sensor would lead to direct improvements in the accuracy of retrieved temperatures. Such improvements were included in the ATSR design and on-orbit performance manifested desired increases in SST retrieval accuracy. ATSR posited validation of the "skin" temperature rather than the "bulk" temperature, as in AVHRR, i.e., validation of the actual sensed parameter in lieu of a surrogate. Preliminary results from ATSR [90], [99] suggest that such is feasible and does add information of geophysical importance.

Design Innovations in the Infrared bands

MODIS incorporates a split-window in the 4μm window with high performance detectors (see Table 5). Addition of this split-window is expected to markedly improve nighttime surface temperature estimates in tropical and sub-tropical regimes, as both channels are transmissive enough to see through maximum column water vapor loads (Figure 8). Addition of bands in the near-infrared (see [9]) permits improvement of cirrus cloud detection and should also provide aerosol detection and absorption estimates. The presence of aerosols, both tropospheric and stratospheric, can introduce unacceptable errors in surface temperature retrievals of >1K [39], [88]. Unless the aerosol layer is sufficiently dense for it to be identified by the cloud screening algorithms, the aerosol effects can not be easily identified in current satellite data themselves. However, MODIS offers for the first time collocated visible-NIR measurements, in which aerosol signatures can be more readily

identified, with the infrared bands used for SST measurements. Thus the combination of infrared data and visible aerosol estimates provided by a single instrument, which has been impractical on previous instruments, will be straightforward on MODIS.

On-orbit characterization of the infrared bands

The state-of-the-art "Denton" coated scan mirror utilized in MODIS to minimize polarization effects in the visible has notable changes in emissivity over the infrared spectral range of the instrument. Characterization of this emissivity to desired levels of accuracy is impractical on earth. The GOES 8 and 9 imagers use similar technology and have developed an on-orbit approach to characterizing mirror emissivity, which is based on deep-space scans [104]. This will also be the approach for determination of MODIS scan mirror infrared emissivity variations.

Algorithm Description

Given well-calibrated radiance's from MODIS, deriving accurate sea surface temperature fields and associated statistics is dependent on the ability to correct for the effects of the intervening atmosphere on these spectral radiance's and to provide assimilation mechanisms which cover the time-space windows of interest. Sensing SST through the atmosphere in the thermal infrared is subject to several environmental factors which degrade the accuracy of the perceived temperature. Major sources of error in the radiometric determination are (a) sun glint (MODIS channels 20, 22, and 23), (b) water vapor absorption in the atmosphere (primarily MODIS channels 31, 32), (c) trace gas absorption (all channels) and (d) episodic variations in aerosol absorption due to volcanic eruptions, terrigenous dust blown out to sea, etc. (all channels). Although satellite radiometers sense the ocean's radiation temperature known as "skin" temperature, satellite results are commonly compared with bulk temperature measurements in the upper several meters of the ocean. Air-sea interaction modifies the relationship between these two

variables and causes observable differences in the bulk and radiation temperatures [30], [93], [97]. We must be prepared to quantify regional and temporal differences between bulk and skin temperatures. This is one of the goals of the *in situ* SST calibration and validation activity.

The integrated atmospheric transmissivity over each of the MODIS infrared channels (20, 22, 23, 31, 32) differs. Consequently, algorithms can be constructed which depend on the differences in measured temperature among these channels [3]. The simplest such algorithm assumes that, for small cumulative amounts of water vapor, the atmosphere is sufficiently optically thin that the difference between the measured temperature in any channel and the true surface temperature can be parmeterized as a simple function of the difference between the measured temperatures in two channels with different atmospheric transmissions.

We are using the line-by-line numerical radiative transfer code developed at Rutherford Appleton Laboratory in the UK as a basis for modeling atmospheric absorption processes in the MODIS infrared bands: [78], [106]. Linear algorithms (MCSST) are

based on a formula of the following form for the surface temperature T_s:

$$T_s = \alpha + \beta T_i + \gamma (T_i - T_j) \qquad (7)$$

where the $T_{i,j}$'s are brightness temperatures in various channels for a given location and the coefficients α, β, and γ give the parameterized correction [33], [78], or can be derived empirically from good composite sets of surface and satellite observations [82]-[84], [93]. In Eq. (7) such an algorithm constructed on channels 31 and 32 would replace i,j by 31, 32 respectively. Although Eq. (7) is easy to implement, it does not permit correction for changes in air mass due to scan-angle. Llewellyn -Jones *et al*., [78] develop a table from numerical simulations which permits modification of Eq. (7) into a form:

$$T_s = \_'(\_) + \_'(\_)\, T_i + \_'(\_)\, (T_i - T_j) \qquad (8)$$

where θ is the zenith angle. This approach reduces the errors at large scan angles for moist atmospheres by more than 1K. Somewhat more complex algorithms have evolved to take into account non-linearities in the radiative transfer, and changing path length effects across the swath of an imaging radiometer. The currently operational atmospheric correction algorithm is the Non-Linear SST (NLSST) equation, [102]-[103],

$$SST = \_ + \_ T_i + \_(T_i - T_j).Ts + \_(T_i - T_j).(\sec\_ - 1) \qquad (9)$$

where Ts is an a priori estimate of the SST and which is used to scale the atmospheric correction for different environmental regimes, and _ is the satellite zenith angle.
For MODIS SST estimation (proto-algorithm) we will eventually implement a correction equation which is a variation of Eq. (9) for multiple pairs of the available bands. This will

be coupled with an objective criterion based on observed retrieval scatter for a local region to determine which channel combination(s) is(are) used.

Level 3 Spatial and Temporal Binning

An extensive series of quality and conditional flags at the pixel level is maintained through the Level 2 processing stages. Appropriate flags from the Level 1B product and cloud mask are carried forward as well. Additional flags and quality assessment indicators are determined at the granule level. Flag and mask definitions and threshold values are provided in detailed product documentation available through the Goddard Distributed Active Archive Center (GDAAC), and will likely undergo significant tuning in the post-launch evaluation phase. The pixel level flags are used in the space binner and time binner programs to maintain data quality in the Level 3 products, and play an important role in assigning quality in validation match-up data sets. Each Level 3 product (Table 6) is binned according to its own criteria and has a unique set of quality flag values for validation assessment. The general philosophy for binning is to include only the highest quality data available within any time period.

Both SST and Ocean Color products use similar binning strategies. The daily space-binned product forms the basis for longer time period compositing, although adjustments are provided where it is important to maintain quasi-equal representation of temporal periods. Thus, for the primary productivity product input, an annual period is comprised of 46 equally weighted weeks. For ease of access at Level 3, one file (including statistics and combined quality flag results) is created for each product at each time interval. Experience with the SST Pathfinder project showed the importance of maintaining proper temporal context of data for quality assessment [39]; therefore both the preceding and following weekly fields are used to flag outlier values. This approach is carried forward with the bio-optical products as well, and is viewed as most appropriate for the atmospheric and surface reflectance fields.

Data day

Another area where there is significant departure from heritage data products is in the definition of the MODIS data day, which applies to data at Level 3. The definition, and the advantages it confers, is discussed in detail by Evans [See 20, Appendix C]. The data-day concept basically uses an earth-centered frame of reference for demarcation of data observation times, rather than the orbital time on the satellite. In essence, near the date line, data are assigned to the GMT data day at the pixel level, rather than mapping entire scans or granules of data to the date indicated by the satellite clock at the time of observation. This removes some aliasing which has characterized other missions. The advantages of this are that comparisons with in-situ observations are more accurate, and the global data set is constrained to the same daylight date which is important for comparisons with ship-board validation data sets of phytoplankton production. A disadvantage is that data from two days are required to observe nearly synoptic features which extend across the date line, and files from three days must be open while performing space and time binning. In other parts of the world the user will be able to ignore the improved accuracy of data mapping.

SUMMARY

MODIS incorporates significant improvements in radiometric quality and capabilities which result from careful analysis of the results from, and experience gained with, its heritage, precursor sensors. These improvements in requirements and instrument specifications for ocean requirements have been challenging, such as SNR, thermal NEDT, and radiometric accuracy, but have a firm basis in both theory and practice. They are coupled with commensurate or greater improvements in algorithms for standard ocean product accuracy and design, which should therefore provide significant enhancements in the ability to observe key oceanic properties and their variability as related to role of the ocean, and response of oceanic ecosystems, to climate variations. Coupled with these new and improved capabilities in the space and data segments, is the requirement for improvements in product validation and assessment of uncertainty fields for the new

products. Significant progress has been made in these areas as well over the past decade, in preparation for SeaWiFS and MODIS validation phases, and is already bearing fruit. Full treatment is beyond the scope of this paper, but significant improvements in our ability to assess uncertainties in water leaving spectral radiance (to on order of ± 1-2%) and SST brightness temperatures (to less than ± 0.2 K) by independent shipboard measurements are in now in hand. Therefore, we have some confidence that the global ocean observational time series begun by MODIS should provide important oceanographic advances both in both the near term, and for future long term studies.

REFERENCES

[1] M. R. Abbott and Letelier R.M., "Going with the flow," in *Monitoring Algal Blooms: New techniques for detecting large-scale environmental changes*, edited by Mati Kahru, Landes Bioscience, Georgetown, *in press*, 1997.

[2] J. Aiken, G. F. Moore, CC. Trees, S. B. Hooker, and D.K. Clark, "The SeaWiFS CZCS-Type Pigment Algorithm," *NASA Technical Memorandum 104556*, Vol 29, S. B. Hooker and E. R. Firestone, Eds. NASA Goddard Space Flight Center, Greenbelt, MD, 34 pp., 1995.

[3] D. Anding and R. Kauth, "Estimation of Sea Surface Temperature from Space," *Remote Sensing of the Environment*, vol. 1, pp. 217-220, 1970

[4] W. M. Balch, R. Evans, J. Brown, G. Feldman, C. McClain, W. Esaias , "The remote sensing of ocean primary productivity: Use of a new data compilation to test satellite algorithms," *Journal of Geophysical Research* , vol. 79, pp. 2279-293, 1992.

[5] W. M. Balch, K. A. Kilpatrick, P. M. Holligan and C. Trees, "The 1991 coccolithophore bloom in the central north Atlantic I - Optical properties and factors affecting their distribution," *Limnology andOceanography*, vol. 41, pp. 1669-1683, 1996.

[6] W. M. Balch, K. Kilpatrick, P. M. Holligan, D. Harbour, and E. Fernandez, "The 1991 coccolithophore bloom in the central north Atlantic II - Relating optics to coccolith concentration," *Limnology and Oceanography*, vol. 41, pp. 1684-1696, 1996.

[7] R. A. Barnes, W. L. Barnes, W. E. Esaias, and C. R. McClain, "Prelaunch Acceptance Report for the SeaWiFS Radiometer.," *NASA Technical Memorandum 104556*, Vol 22, S. B. Hooker, E. R. Firestone and J. A. Acker, Eds. NASA Goddard Space Flight Center, Greenbelt, MD, 32 pp. 1994.

[8] R. A. Barnes, A.W. Holmes, W. L. Barnes, W. E. Esaias, C. R. McClain, and T. Svitek, "SeaWiFS Prelaunch Radiometric Calibration and Spectral Characterization," *NASA Technical Memorandum 104556*, Vol 23, S. O. B. Hooker, E. R. Firestone and J. A. Acker, Eds. NASA Goddard Space Flight Center, Greenbelt, MD, 55 pp., 1994.

[9] W. L. Barnes, T. Pagano, V. V. Salomonson, "Prelaunch Characteristics of the Moderate Resolution Imaging Spectroradiometer (MODIS) on EOS AM-1 ," submitted *IEEE Trans. Geosci. Remote Sens.*, (this issue) vol. 00,000-000, 1998.

[10] I. J. Barton, A.J. Prata, and D.T. Llewellyn-Jones, "The Along Track Scanning Radiometer–an Analysis of coincident ship and satellite measurements," *Adv. Space Res.*, vol. 13, n. 5, pp. 69, 1993.

[11] I.J. Barton, M. Zavody, D.M. O'Brien, D.R. Cutten, R.W. Saunders and D.T. Llewellyn-Jones, "Theoretical algorithms for satellite-derived sea surface temperatures," *J. Geophys. Res.*, vol. 94, p. 3365, 1989.

[12] M. J. Behrenfeld and P. G. Falkowski, "Photosynthetic rates derived from satellite-based chlorophyll concentration," *Limnology and Oceanography*, vol. 42, pp. 1-20, 1997.

[13] R. R Bidigare, M. E. Ondrusek, J. H. Morrow, D. A. Kiefer, In vivo absorption properties of algal pigments, *SPIE Vol. 1302 Ocean Optics X* ,pp. 290-302, 1990.

[14] W.P. Bissett, J. Patch, K.L. Carder, and Z.P. Lee, "Spectrophotometric determination of pigment packaging in high light, oceanic surface waters for remote sensing algorithms to estimate phytplankton biomass" (submitted to Limnology and Oceanography).

[15] A. Bricaud, A. Morel, and L. Prieur, "Absorption by dissolved organic matter in the sea (yellow substance) in the UV and visible domains," *Limnologoy and Oceanography*, vol. 26, pp. 43-53, 1981.

[16] J. T. Bradshaw and H.E. Fuelberg, "An evaluation of HIS interferometer soundings and their use in mesoscale analysis," *J. Appl. Meteor*., vol. 32, pp. 522-538, 1993.

[17] C. W. Brown, "Classification of Coccolithophore Blooms in Ocean Color Imagery,". Chapter 3 in *SeaWiFS Algorithms, Part 1. NASA Technical Memorandum 104556*, Vol 28, S. B. Hooker, E. R. Firestone and J. A. Acker, Eds. NASA Goddard Space Flight Center, Greenbelt, MD, 38 pp. 1995.

[18] C. W. Brown and J. A. Yoder, "Coccolithophorid blooms in the global ocean," *J. Geophys. Res.*, vol. 99, pp 7467-7482, 1994.

[19] W. L. Butler, "Energy distribution in the photochemical apparatus of photosynthesis," *Ann. Rev. Plant Physiol.*, vol. 29, pp. 345-378, 1978.

[20] J. W. Campbell, J. M. Blaisdell and M. Darzi, "Level-3 SeaWiFS Data Products: Spatial and Temporal Binning Algorithms," *NASA Technical Memorandum 104566*, vol 32, 63pp. 1995.

[21] D. G. Capone, D.G., J.P. Zehr, H.W. Paerl,B. Bergman, and E.J. Carpenter, " *Trichodesmium*, a globally significant marine cyanobacterium," *Science*, vol. 276, pp. 1221-1229, 1997.

[22] K. L. Carder, S. K. Hawes, Z. Lee, and F. R. Chen, MODIS Ocean Science Team ATBD, Case 2 Chlorophyll *a*, Version 4, 1997a.

[23] K. L. Carder, S. K. Hawes, Z. Lee, and F. R. Chen, MODIS Ocean Science Team ATBD, Instantaneous Photosynthetically Available Radiation and Absorbed Radiation by Phytoplankton, Version 4, 1997b.

[24] K. L. Carder, S.K. Hawes, and Z.P. Lee. 1996. SeaWiFS Algorithm for Chlorophyll *a* and Colored Dissolved Organic Matter in Subtropical Environments, (submitted to J. G. R.).

[25] R. J. Charleson, J. E. Lovelock, M. O. Andreae, and S. G. Warren, "Oceanic phytoplankton, atmospheric sulfur, cloud albedo, and climate," *Nature*, vol. 326, pp 655-661, 1987.

[26] W. S. Chamberlin and J. Marra, "Estimation of photosynthetic rate from measurements of natural fluorescence: Analysis of the effects of light and temperature," *Deep Sea Res.*, vol. 39, pp.1695-1706, 1992.

[27] W. S. Chamberlin, C. R. Booth C.R., Kiefer D.A., Morrow J.H., and Murphy C.R., "Evidence for a simple relationship between natural fluorescence, photosynthesis and chlorophyll in the sea," *Deep-Sea Res.*, vol. 37, pp. 951-973, 1990.

[28] D. K. Clark "Phytoplankton algorithms for the Nimbus-7 CZCS," in *Oceanography From Space* , JFR Gower, Ed., pp. 227-238. Plenum Press, New York, 1981.

[29] D. K. Clark, H. R. Gordon, K. J. Voss, Y. Ge, W. Broenkow, and C. Trees, "Validation of Atmospheric Correction Over the Oceans," *J Geophys. Res.* (in press), 1997.

[30] P. Cornillon and L. Stramma, "The distribution of diurnal sea surface warming events in the western Sargasso Sea," *J. Geophys. Res.*, vol. 98C, n. 6, pp. 11811-11815, 1985.

[31] C. Cox and W. Munk, "Measurements of the roughness of the sea surface from photographs of the Sun's glitter," *J. Opt. Soc. Am.*, vol. 44, pp. 838-850, 1954.

[32] M. E. Culver and M. J. Perry, "Detection of phycoerythrin fluorescence in upwelling irradiance spectra," *Eos Trans. AGU*, vol. 75, p. 233, 1994.

[33] P. Y. Deschamps and T. Phulpin, "Atmospheric corrections of infrared measurements of sea surface temperature using channels at 3.7 µm, 11 µm and 12 µm," *Boundary Layer Meteor.* vol. 18, pp. 131-143, 1980.

[34] R. C. Dugdale and J.J. Goering, "Uptake of new and regenerated forms of nitrogen in primary productivity". *Limnolology and Oceanography* , vol. 12, pp. 196-206, 1967.

[35] T. Edwards, R. Browning, J. Delderfield, D. J. Lee, K. A. Lidiard, R. S. Milborrow, P. H. McPherson, S. C. Peskett, G. M. Toplis, H. S. Taylor, I. Mason, G. Mason, A. Smith and S. Stringer, "The Along Track Scanning Radiometer - Measurement of sea-surface temperature from ERS-1," *Journal of the British Interplanetary Society*, vol. 43, pp. 160- 1990.

[36] W. E. Esaias, R. Iverson, and K. Turpie, **"**Ocean province classification using ocean color data: observing biological signatures of variations in physical dynamics**,"** *Global Change Biology*, submitted Nov. 1997.

[37] W. E. Esaias, "Remote sensing of oceanic phytoplankton: Present capabilities and future goals," In *Primary Productivity in the Sea*, P. G. Falkowski, Ed, pp. 321-337 Plenum, New York, 1980.

[38] R. L Evans and H. R. Gordon, "CZCS 'System Calibration:' A retrospectiveexamination," *J.Geophys. Res.* vol. 99, pp 7293-7307, 1994.

[39] R. H. Evans and G. Podestá, "AVHRR Pathfinder: SST Approach and Results," AGU Fall meeting, San Francisco, CA. *EOS Transactions*, vol. 77, p. 46, F354, 1996.

[40] P. G. Falkowski and Z. Kolber, "Estimation of phytoplankton photosynthesis by active fluorescence," *ICES mar. Sci. Symp.*, vol. 197, pp. 92-103, 1993.

[41] P. G. Falkowski and The Ocean Primary Productivity Working Group, "Using satellite data to derive primary productivity in the world oceans," submitted for publication in *NASA Technical Memorandum 104556*, Vol 36, S. B. Hooker and E. R. Firestone, Eds. NASA Goddard Space Flight Center, Greenbelt, MD, 1997.

[42] G. C. Feldman, W. Esaias, C. McClain, J. Elrod, N. Maynard, D. Endres, "Ocean Color: Availability of the global data set," *EOS Trans. Am. Geo. U.*, vol. 70, pp. 634-641, 1989.

[43] J. Fischer and U. Kronfeld, "Sun-stimulated chlorophyll fluorescence 1: Influence of oceanic properties," *Int. J. Remote Sensing*, vol. 11 pp. 2125-2147, 1990.

[44] R. Frouin, M. Schwindling, and P.Y. Deschamps, "Spectral reflectance of sea foam in the visible and near-infrared: In-situ measurements and implications for remote sensing of ocean color and aerosols," *Jour. Geophys. Res.*, vol. 101C, pp. 14,361-14,371, 1996.

[45] H.R. Gordon, "Removal of Atmospheric Effects from Satellite Imagery of the Oceans," *Applied Optics*, vol. 17, pp. 1631-1636 ,1978.

[46] H. R. Gordon, "Diffuse reflectance of the ocean: the theory of its augmentation by chlorophyll *a* fluorescence at 685 nm," *Appl. Opt.* vol. 18, pp. 1161-1166, 1979.

[47] H.R. Gordon, "Atmospheric Correction of Ocean Color Imagery in the Earth Observing System Era," *Jour. Geophys. Res.*, vol. 102D, 17,081-17,106, 1997.

[48] H.R. Gordon, J.W. Brown, R.H. Evans, "Exact Rayleigh Scattering Calculations for use with the Nimbus-7 Coastal Zone Color Scanner," *Applied Optics*, vol. 27, pp. 862-871, 1988.

[49] H.R. Gordon, O.B. Brown, R.H. Evans, J.W. Brown, R.C. Smith, K.S. Baker, and D.K. Clark, "A Semi-Analytic Radiance Model of Ocean Color," *Jour. Geophys. Res.*, vol. 93D, pp. 10909-10924, 1988.

[50] H.R. Gordon and D.K. Clark, "Atmospheric Effects in the Remote Sensing of Phytoplankton Pigments," *Boundary Layer Meteorology*, vol. 18, pp. 299-313, 1980.

[51] H.R. Gordon, D.K. Clark, J.L. Mueller, and W.A. Hovis, "Phytoplankton Pigments Derived from the Nimbus-7 CZCS: Initial Comparisons with Surface Measurements," *Science*, vol. 210, pp. 63-66, 1980.

[52] H.R. Gordon and D.K. Clark, "Clear water radiances for atmospheric correction of Coastal Zone Color Scanner imagery," *Applied Optics*, vol. 20, pp. 4175-4180, 1981.

[53] H.R. Gordon, D.K. Clark, J.W. Brown, O.B. Brown, R.H. Evans, and W.W. Broenkow, "Phytoplankton Pigment Concentrations in the Middle Atlantic Bight: Comparison of Ship Determinations and Coastal Zone Color Scanner Measurements," *Applied Optics*, vol. 22, pp. 20-36, 1983.

[54] H.R. Gordon, T. Du, and T. Zhang, "Remote sensing ocean color and aerosol properties: resolving the issue of aerosol absorption," *Applied Optics*, in press, vol. 36, 0000-0000, 1997.

[55] H.R. Gordon and A.Y. Morel, *Remote Assessment of Ocean Color for Interpretation of Satellite Visible Imagery: A Review*, Springer--Verlag, New York 114 pp. 1983.

[56] H.R. Gordon and M. Wang, "Influence of Oceanic Whitecaps on Atmospheric Correction of SeaWiFS, *Applied Optics*," vol. 33, pp. 7754-7763 1994a.

[57] H.R. Gordon and M. Wang, "Retrieval of water-leaving radiance and aerosol optical thickness over the oceans with SeaWiFS: A preliminary algorithm," *Applied Optics*, vol. 33, pp. 443-452, 1994.

[58] J.F.R. Gower and G.A. Borstad, "Mapping of phytoplankton by solar-stimulated fluorescence using an imaging spectrometer," *Int. J. Remote Sensing*, vol. 11 pp. 313-320, 1990.

[59] W. W. Gregg, "Analysis of Orbit Selection for SeaWiFS: Ascending vs Descending Node," *NASA Technical Memorandum 104556*, Vol 2, S. B. Hooker and E. R. Firestone, Eds. NASA Goddard Space Flight Center, Greenbelt, MD, 16 pp. 1992.

[60] W. W. Gregg and K. L. Carder, "A simple spectral solar irradiance model for cloudless maritime atmospheres," *Limnology and Oceanography* , vol. 35, n. 8, pp. 1657-1675, 1990.

[61] W. W. Gregg and R. H. Woodward, "Improvements in coverage frequency of ocean color: Combining data from SeaWiFS and MODIS" *IEEE Trans. Geosci. Remote Sens.*, (this issue) vol. 00,000-000, 1998.

[62] B. Guenther, W. Barnes, E.Knight, J.Barker, J.Harnden, R.Weber, M.Roberto, G.Godden, H.Montgomery, and P.Abel, "Modis Calibration: A Brief Review of the Strategy for the At-Launch Calibration Approach," *J.Atmos. Oce. Technol*., vol. 13, n. 2, pp. 274-285, 1996.

[63] F. E. Hoge and R. N. Swift. "Airborne simultaneous spectroscopic detection of laser-induced water-Raman backscatter and fluorescence from chlorophyll a and other naturally occurring pigments", *Appl. Opt*. vol. 20, pp. 3197- 3205, 1981.

[64] F. E. Hoge, and R. N. Swift. "Active-passive correlation spectroscopy: A new technique for identifying ocean color algorithm spectral regions", *Appl. Opt*. vol. 25, pp. 2571-2583, 1986.

[65] F. E. Hoge and R. N. Swift, "Phytoplankton Accessory Pigments: Evidence for the Influence of Phycoerythrin on the Submarine Light Field", *Remote Sensing of Environment*, vol. 34, pp. 19-25, 1990.

[66] F. E. Hoge, and Paul E. Lyon, "Satellite Retrieval of Inherent Optical Properties by Linear Matrix Inversion of Oceanic Radiance Models: An Analysis of Model and Radiance Measurement Errors," *Jour. Geophys. Res*. vol. 101, pp. 16,631-48, 1996.

[67] P. M. Holligan, E. Fernandez, J. Aiken, W. M. Balch, P. Boyd, P. H. Burkhill, M. Finch, S. B. Groom, G. Malin, K. Muller, D. A. Purdie, C. Robinson, C. C. Trees, S. M. Turner, and P. van der Wal, "A biogeochemical study of the coccolithophore *Emiliana huxleyi* in the North Atlantic," *Global Biogeochemical Cycles*, vol. 7, pp. 879-900, 1993.

[68] K. L . Howard, *Estimating global ocean primary production using satellite-derived data*. Master's Thesis, 98 pp. University of Rhode Island. 1995.

[69] R. L. Iverson and W. Esaias, "Ocean Phytoplankton Total Carbon and New Production, and Export Production Estimated Using Empirical Equations and CZCS Data," *Global Change Biology*, (submitted November,1977).

[70] JGOFS Photosynthesis Measurements Task Team, "Measurement of the parameters of photosynthesis: Light absorption and quantum yield of photosynthesis derived from P vs E determinations," *J. Plankton Res*. (In Press) 1997.

[71] D. Kamykowski, "A preliminary biophysical model of the relationship between temperature and plant nutrients in the upper ocean," *Deep Sea Res*., vol. 34 n. 7, pp 1067-1079, 1987.

[72] D. M. Karl, R. Letelier, D. Hebel, L. Tupas, J. Dore, J. Christian, and C. Winn, "Ecosystem changes in the North Pacific subtropical gyre attributed to the 1991-92 El Nino." *Nature,* vol. 373, pp. 230-234, 1995.

[73] D.A. Kiefer, W.S. Chamberlin, and C.R. Booth, "Natural fluorescence of chlorophyll *a*: Relationship to photosynthesis and chlorophyll concentration in the western South Pacific gyre," *Limnol. Oceanogr*., vol. 34, pp. 868-881, 1989.

[74] M. Kishino, S. Sugihara, and N. Okami, "Influence of fluorescence of chlorophyll *a* on underwater upward irradiance spectrum," *La Mer*, vol. 22, pp. 224-232, 1984.

[75] Z. Lee, K. L. Carder, S. K. Hawes, R. G. Steward, T. G. Peacock, and C. O. Davis, "A model for interpretation of hyperspectral remote-sensing reflectance," *Appl. Opt.*, vol. 33, pp. 5721-5732, 1994.

[76] R. M. Letelier and M. R. Abbott, "An analysis of chlorophyll fluorescence algorithm for the Moderate Resolution Imaging Spectrometer (MODIS)," *Remote Sens. Environm.*, vol. 58, pp. 215-223, 1996.

[77] R. M. Letelier, M.R. Abbott, and D.M. Karl, Chlorophyll natural fluorescence response to upwelling events in the Southern Ocean, *Geophys. Res. Letters*, vol. 24, pp. 409-412, 1997.

[78] D.T. Llewellyn-Jones, P.J. Minnett, R.W. Saunders and A.M. Zavody, "Satellite multichannel infrared measurements of sea surface temperature of the N.E. Atlantic Ocean using AVHRR/2," *Quart. J. R. Met. Soc.* vol. 110, pp. 613-631, 1984.

[79] A. Longhurst, S. Sathyendranath, T. Platt, C. Caverhill, An estimate of global primary production in the ocean from satellite radiometer data. *Journal of Plankton Research* , vol. 17 pp. 1245-1271, 1995.

[80] C. R. McClain, K. R. Arrigo, W. E. Esaias, M. Darzi, F. S. Patt, R. H. Evans, J. W. Brown and, R. A. Barnes, and L. Kumar, "SeaWiFS Algorithms, Part 1," *NASA Technical Memorandum 104556*, Vol 28, S. B. Hooker, E. R. Firestone and J. A. Acker, Eds. NASA Goddard Space Flight Center, Greenbelt, MD, 38 pp., 1995.

[81] C. R. McClain, G. C. Feldman, and, W. E. Esaias, "Oceanic biological productivity," in *Atlas of Satellite Observations Related to Global Change*, R. Gurney, J. L. Foster, and C. L. Parkinson, Eds., Cambridge Univ. Press, pp. 251-263, 1993.

[82] E. P. McClain, "Multiple atmospheric -- window techniques for satellite derived sea surface temperatures," Chapter 13 in *Oceanography from Space*, J.F.R. Gower, ed., Plenum, New York. 1981.

[83] E. P. McClain, W.G. Pichel, C.C. Walton, Z. Ahmed, and J. Sutton, "Multi-channel improvements to satellite derived global sea surface temperatures," Proc. XXIV COSPAR, *Advances Space Res*. vol. 2, pp. 43-47, 1983.

[84] E. P. McClain, W.G. Pichel and C.C. Walton, "Comparative performance of AVHRR-based multichannel sea surface temperatures," *J. Geophys. Res*., vol. 90C, pp. 11587-11601, 1985.

[85] P.J. Minnett, "Satellite infrared scanning radiometers - AVHRR & ATSR," In *Microwave Remote Sensing for Oceanographic and Marine Weather-Forecast Models,* R.A. Vaughn, ed. Kluwer Academic Publishers. 1990.

[86] P.J. Minnett, "Sea surface temperature measurements from the Along-Track Scanning Radiometer on ERS-1," in *Oceanographic Applications of Remote Sensing*, M. Ikeda and F. Dobson, Eds., CRC Press Inc. 131-143. 1995a.

[87] P.J. Minnett, "The Along-Track Scanning Radiometer: Instrument Details," In *Oceanographic Applications of Remote Sensing*, M. Ikeda and F. Dobson, Eds., CRC Press Inc. 461-472. 1995b.

[88] P.J. Minnett, and R.H. Evans, "Evidence of Effects of Aerosols on Thermal Infrared Measurements from Satellites," *Proceedings 2nd ARM Aerosol Workshop*, Oak Ridge National Laboratory, November 1996.

[89] J. L. Mueller and R. W. Austin, "Ocean Optics Protocols for SeaWiFS Validation, Revision 1," *NASA Technical Memorandum 104556*, Vol 25, S. B. Hooker, E. R. Firestone and J. A. Acker, Eds. NASA Goddard Space Flight Center, Greenbelt, MD, 66 pp., 1995.

[90] C.T. Mutlow, D.T. Llewellyn-Jones, A.M. Závody and I.J. Barton, "Sea surface temperature measurements by the Along-Track Scanning Radiometer on the ERS-1 Satellite: Early results," *J. Geophys. Res*. vol. 99, pp. 22,575-22,588, 1994.

[91] R.A. Neville and J.F.R. Gower, "Passive remote sensing of phytoplankton via chlorophyll a fluorescence," *J. Geophys. Res*., vol. 82C, pp. 3487-3493, 1977.

[92] J. R. O'Reilly and S. Maritorena, "Ocean Color Chlorophyll Algorithms forSeaWiFS," J. Geophys. Res. (Submitted Sept. 1997).

[93] Prabhakara, C., G. Dalu and V.G. Kunde, 1974. Estimation of Sea Surface Temperature from remote sensing in the 11 µm to 13 µm window region. J. Geophys. Res. 79(12), 1744-1749.

[94] I. S. Robinson, N. C. Wells, and H. Charnock, "The sea surface thermal boundary layers and its relevance to the measurement of sea surface temperature by airborne and space borne radiometers," *Int. J. Remote Sens.*, vol. 5, pp, 19-46, 1984.

[95] V. V. Salomonson, W. L. Barnes, P. Maymon, H. E. Montgomery, and H. Ostrow, "MODIS: Advanced Facility Instrument for Studies of the Earth as a System," *IEEE Trans. Geosci. Remote Sens*., vol. 27 n. 2, 145-153, 1989.

[96] J. L. Sarmiento and C. Le Quere C, "Oceanic carbon dioxide uptake in a model of century-scale global warming," *Science*, vol. 274, pp. 1346-1350, 1996.

[97] P. Schluessel, W.J. Emery, H. Grassl and T. Mammen, "On the bulk-skin temperature difference and its impact on satellite remote sensing of sea surface temperatures," *J. Geophys. Res.*, vol. 95, pp. 13,341-13,356, 1990.

[98] A. Schwalb, "Modified version of the improved TIROS operational satellite (ITOS D-G)," *NOAA TM NESS 35*. Available from NTIS as COM-72-10547, 48 pp., 1973.

[99] A. Schwalb, "The TIROSN/NOAA A-G satellite series," *NOAA TM NESS* 95, available from NTIS, 75 pp., 1978.

[100] E.P. Shettle and R.W. Fenn, "Models for the Aerosols of the Lower Atmosphere and the Effects of Humidity Variations on Their Optical Properties", *Air Force Geophysics Laboratory, Hanscomb AFB, MA 0173, No. AFGL-TR-79-0214*, 1979.

[101] A.H. Smith, R.W. Saunders and A.M. Závody, "The validation of ATSR using aircraft radiometer data over the Tropical Atlantic," *J. Atmos. and Oceanogr. Techn.* vol. 11, pp. 789-800, 1994.

[102] C. C. Walton, "Nonlinear multichannel algorithms for estimating sea-surface temperature with AVHRR satellite data," *J. Appl. Meteor.* vol. 27, pp. 115-124, 1988.

[103] C. C. Walton, E.P. McClain and J.F. Sapper, "Recent changes in satellite-based multi-channel sea surface temperature algorithms," *Preprint, Marine Technology Society Meeting, MTS '90*, Marine Technology Society, Washington DC, September 1990.

[104] M. Weinreb, "Real-world calibration of GOES -8 and -9 sensors," In *GOES -8 and Beyond* Proc SPIE Intl. Symposium on Optical Science, Engineering and Instrumentation. Denver, CO., 4-9 Aug, 1996., E.R. Washell, Ed. pp. 888, 1996.

[105] J. A. Yoder, C. R. McClain, G. C. Feldman, and W. E. Esaias, "Annual cycles of phytoplankton chlorophyll concentrations in the global ocean: A satellite view," *Global Biogeochem.* Cycles, vol. 7, pp. 181-193, 1993.

[106] Zavody, A.M., C.T. Mutlow, and D.T.Llewellyn-Jones, “A radiative transfer model for sea surface temperature retrieval for the Along-Track Scanning Radiometer,” *J. Geophys. Res.*, vol. 100, pp. 937-, 1995.

FIGURE CAPTIONS

Figure 1. Upwelling radiance at the top of atmosphere and at the ocean surface for extremely low and very high oceanic chlorophyll a concentrations. (4 lines from top to bottom on left are: TOA- 0.01 mg/m^3, TOA- 10 mg/m^3, surface- 0.01 mg/m^3, and surface, 10 mg/m^3). Model radiances simulate a nadir view at 60 degree solar zenith angle, or a clear atmosphere with an aersosol optical depth at 670 nm of 0.2, Angstrom exponent of 0.5, 5 mm precipitable water, and 0.35 cm ozone. Measured values of Noise Equivalent delta Radiance (NEDL) for MODIS bands 8-16 are shown as bars.

Figure 2. SNR for CZCS, SeaWiFS, and MODIS, computed at a standard input radiance value, from Table 1. SNR in 4 MODIS high resolution bands (1-4) is also indicated. Values are plotted at band centers.

Figure 3. MODIS Ocean Color Level 2 Simplified Algorithm Flow diagram. Geophysical products are at arrow terminations.

Figure 4. Performance of the combined empirical (diamonds) and semi-analytic (plus signs) chlorophyll algorithms for global in-situ observations, predicted using the MODIS algorithm from shipboard optical observations (Global Unsorted), and from regions where phytoplankton “packaging” effects are important (Packaged) and negligable (Unpackaged). RMS difference is given in terms of log chlorophyll.

Figure 5. Illustration of the approach for determining the baseline and Fluorescence Line Height at 678 nm, using bands 13, 14, and 15.

Figure 6. Ocean Primary Productivity AlgorithmFlow Diagram, illustrating the short term Productivity Index and Annual HV pathways.

Figure 7. Earth radiance in the mid- to far-infrared spectrum. The various curves give a range of expected infrared radiances for a variety of typical atmospheres and surface temperatures. A 300K blackbody curve is provided to permit visual comparison of the path

length absorption for the various cases. Profile data is computed by the Lowtran radiative transfer program [Selby et al., 1978].

Tables

1. Input Radiances and Signal to Noise Ratios for ocean bands on U.S. ocean color sensors. SNRspec and SNR actual are at Lin,spec. SNR model is adjusted to model top of atmosphere (TOA) radiance for 10 mg/m3 chlorophyll a, (see Figure 1). Wavelength un its are nm at the nominal band centers, radiance units are W m^{-2} μ^{-1} sr^{-1}.

2. MODIS Level 2 Ocean products, showing the relationship to MODIS Product Identification numbers and Algorithm Theoretical Basis Document numbers.

3. Preliminary At-Launch values of Coefficients for Equations 3 and 4.

4. Band characteristics of satellite-borne infrared radiometers.

5. Bands for MODIS Infrared SST Determinations.

6. Table of Level 3 Product Files. Files contain the sum, sum squared, numbers of observations, and pixel level quality assessment information, and will be for daily, 8 day, monthly, and annual time periods at 4.2 x 4.2 km, and 1x1 degree spatial resolution. ESDT is the Earth Science Data Type used by the Goddard DAAC.

TABLES

Band	Wavelength	$L_{in,spec}$	SNR_{spec}	SNR_{actual}	$L_{TOA\ model}$	SNR_{model}
		CZCS				
1	443	54.10	150	260	40.60	211
2	520	35.00	140	260	23.34	180
3	550	28.60	125	233	20.23	208
4	670	13.40	100	143	9.79	112
		SeaWiFS				
1	412	91.00	499	940	47.80	623
2	443	84.10	674	950	40.60	640
3	490	65.60	667	1156	29.89	651
4	510	54.40	640	1055	26.50	659
5	555	44.50	596	690	19.38	558
6	670	26.00	442	798	9.79	386
7	758	16.10	455	860	5.96	398
8	865	10.90	467	670	3.56	295
		MODIS				
8	411	44.90	880	933	46.80	956
9	442	41.90	838	1325	40.60	1300
10	487	32.10	802	1308	29.89	1253
11	530	27.90	754	1385	22.70	1224
12	547	21.00	750	1114	19.38	1062
13	665	9.50	910	1163	9.91	1193
14	677	8.70	1087	1265	9.38	1323
15	746	10.20	586	1077	6.22	800
16	866	6.20	516	1000	3.56	717
3	466 (0.5 km)	35.30	243	316	36.44	328
4	553 (0.5 km)	29.00	228	302	19.38	240
1	644 (0.25 km)	21.80	128	168	10.06	114
2	855 (0.25 km)	24.70	201	414	3.56	132

Table 1. Input Radiances and Signal to Noise Ratios for ocean bands on U.S. ocean color sensors.
SNR spec and SNR actual are at Lin, spec.
SNR model is adjusted to model top of atmos. (TOA) radiance
Wavelength units are nm, radiance units are W/m^2/u/sr

Algorithm	Product Handbook ID	Product Handbook Name	Fields	ATBD	PI	Resolultion
Atmospheric Correction	MOD-18	Water Leaving Radiance	Water Leaving Radiance, Atmos. Transmittance, Aerosol Optical Depths, Model Index, Epsilon Values	ATBD-MOD-17	Gordon	1km, DWM
	MOD-37	Ocean Aerosol Properties	Aerosol Optical Depths, Bands 8-16			
Empirical Algorithms	MOD-19	Pigment Concentrations	CZCS pigment, Total Pigment, Case 1 Chlorophyll a	ATBD-MOD-18	Clark	1km, DWM
	MOD-23	Suspended Solids	Suspended Solids Conc.			
	MOD-26	Diffuse Attenuation Coefficient	Diffuse Attenuation Coefficient (k490)			
Semi-analytic Algorithms	MOD-21	Chlorophyll	MODIS Chlorophyll a (Case 1&2)	ATBD-MOD-19	Carder	1km, DWM
	MOD-36	Total absorption coefficient	a_{tot}, a_{ph}, a_{tot}, A_{ph}			
	MOD-24	Organic matter cons.	a_g			
PAR	MOD-22	IPAR	Instantaneous PAR, Abs. Rad. for Photosyn. (ARP)	ATBD-MOD-20	Carder	1km, DWM
Clear-water Epsilons	MOD-39	Epsilons	Epsilons	ATBD-MOD-21	Carder	1km, DWM
Coccolith	MOD-25	Coccoliths	Corrected Pigment, Coccolith conc., Calcite conc.	ATBD-MOD-23	Gordon (Balch)	1km, DWM
Phycobilipigments	MOD-31	Phycoerythrin	PEB, PUB	ATBD-MOD-27	Hoge	1km, DWM
Chlorophyll Fluorescence	MOD-20	Fluorescence	Fluorescence Line Height, Baseline	ATBD-MOD-22	Abbott	2 km, DWM
Primary Production	MOD-27	Primary Production	Weekly Prod. Index, Annual Total Production, Annual Export Production, Annual New Production	ATBD-MOD-24	Esaias	4.5 km, WMY
Sea Surface Temperature	MOD-28	SST	Skin and Bulk Temp, (Day, Night; 11- 12 μ, 4 μ)	ATBD-MOD-25	Brown	1km, DWM
Match-up Validation Data Base	MOD-32	Match-up Data	SST, Bio-optics	ATBD-MOD-26	Evans	5x5 1km arrays

Table 2. Modis Level 2 Ocean Products

Product	A	B	C	D	E	e	f	g
log(Pigment)CZCS	0	0	-1.27	0.5	1	1	0	0
log(Pigment)SeaWiFS	-4.54	10.32	-9.74	3.00	1	1	1	1
log(Chl a)	-4.99	12.34	-12.12	3.78	1	1	1	1
log(Diffuse Attn)	0	0	-1.4	0.07	1	1	0	0

TABLE 3. Preliminary Regression and Band Selection Coefficients for use in the Empirical Bio-Optical Algorithms, Equations 3 and 4.

	MODIS [1]		*AVHRR*[2]		*ATSR*[3]		*OCTS*[4]		*GLI*[5]	
NO.	λ (μm)	NEΔT (K)	λ (μm)	NEΔT (K)	λ (μm)	NEΔT (K)	λ (μm)	NEΔT (K)	λ (μm)	NEΔT (K)
20	3.78	0.028	3.75	0.12	3.7	0.019	3.7	0.15	3.715	<0.15
22	3.97	0.028								
23	4.056	0.026								
29	8.518	0.012					8.52	0.15	8.3	<0.1
31	11.017	0.024	10.5	0.12	10.8	0.028	10.8	0.15	10.8	<0.1
32	12.032	0.04	11.5	0.12	12.	0.025	11.9	0.15	12	<0.1

[1] For Proto-Flight Model., From [9].

[2] For a target temperature of 300K. From Planet, 1988.

[3] Derived from 500 samples of black-body measurement at a temperature of 298K. [From Minnett, 1995b].

[4] For a target temperature of 300K. From OCTS instrument description.

[5] From NASDA Research Announcement , October 24, 1995.

Table 4. Channel characteristics of satellite-borne infrared radiometers

Band Number	Band Center (μ)	Bandwidth (μ)	NEΔT (K)
20	3.785	0.1877	0.0275
22	3.970	0.0876	0.0277
23	4.056	0.0867	0.0255
31	11.0172	0.537	0.0244
32	12.0324	0.525	0.0402

Table 5. Bands for MODIS Infrared SST Determination

ESDT	MODIS Prod ID	Field Description
MODOCX01-07	MOD 18	nLw, 412..678
08	MOD 37	Tau aerosol,865
09	MOD 37	epsilon (765/865)
10-11	MOD 37	Aerosol model ID 1,2
12	MOD 39	epsilon for clear water, 531
13	MOD 19	CZCS Pigment
14	MOD 19	Chlorophyll_MODIS
15	MOD 19	Total pigment - case 1
16	MOD 20	Fluorescence Line Height
17	MOD 20	Fluorescence Baseline
18	MOD 20	Fluorescence Efficiency
19	MOD 23	Suspended Solids Concentration
20	MOD 25	Pigment conc. in coccolith. blooms
21	MOD 25	coccolith concentration
22	MOD 25	calcite concentration
23	MOD 26	Diffuse Attenuation (K_490)
24	MOD 31	Phycoerythrobilin (PEB)
25	MOD 31	Phycourobilin (PUB)
26	MOD 21	Chlorophyll_a (semianalytic)
27	MOD 21	Chlorophyll a (default)
28	MOD 22	Instantaneous PAR
29	MOD 22	Absorbed Radiation by Phyto. (ARP)
30	MOD 24	Gelbstoffe absorption coefficient
31	MOD 36	Chl. a. absorption coefficient
32-36	MOD 36	Total absorption,412..551
MOD27-1	MOD 27	Prim. Prod. Wkly Indexes
MOD27-2	MOD 27	Prim. Prod. Index Ann. Average
MOD27-3	MOD 27	Prim Prod. Annual HV Tot. New, Exp.
MOD28XD1	MOD 28	SST (skin, bulk), Day
MOD28XD2	MOD 28	SST (skin,bulk), Day, 4 microns
MOD28XN1	MOD 28	SST (skin,bulk), Night
MOD28XN2	MOD 28	SST(skin, bulk), Night, 4 microns

TABLE 6. MODIS OCEAN L-3 PRODUCTS

FIGURES

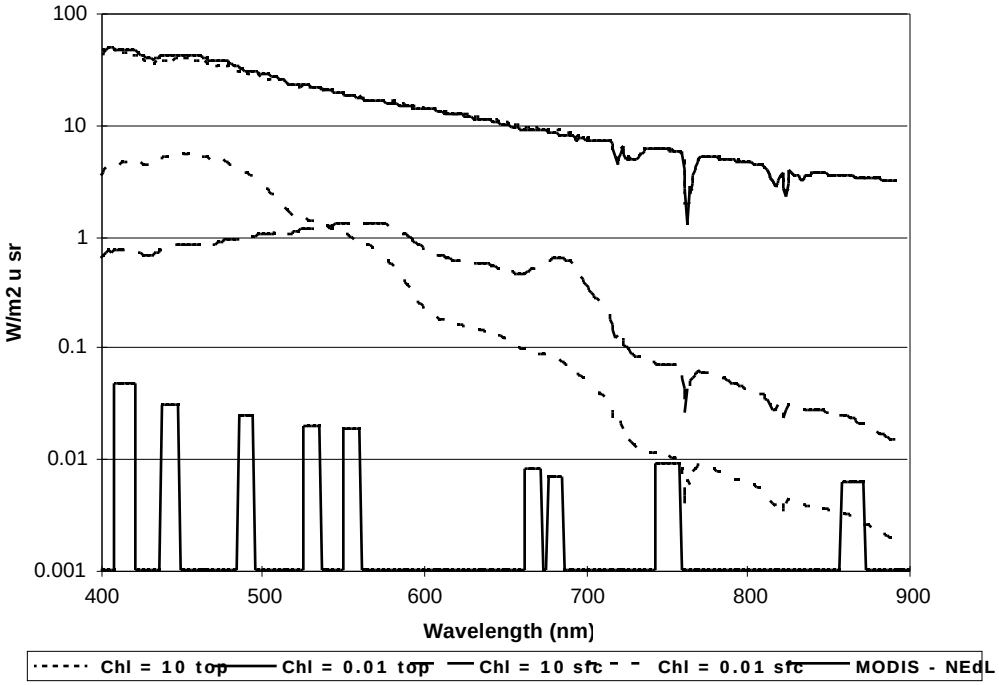

FIGURE 1

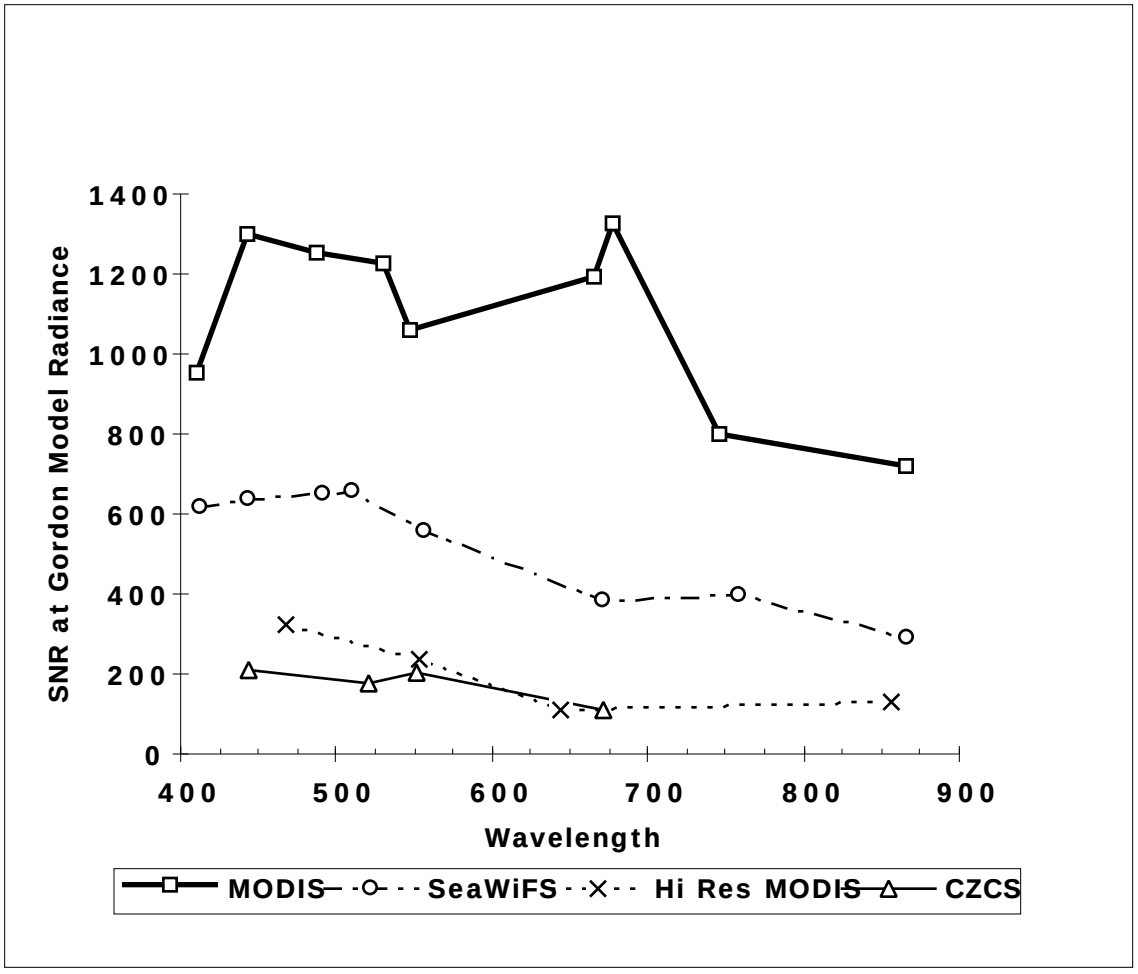

Figure 2. Normalized SNR for U.S. ocean color sensors.

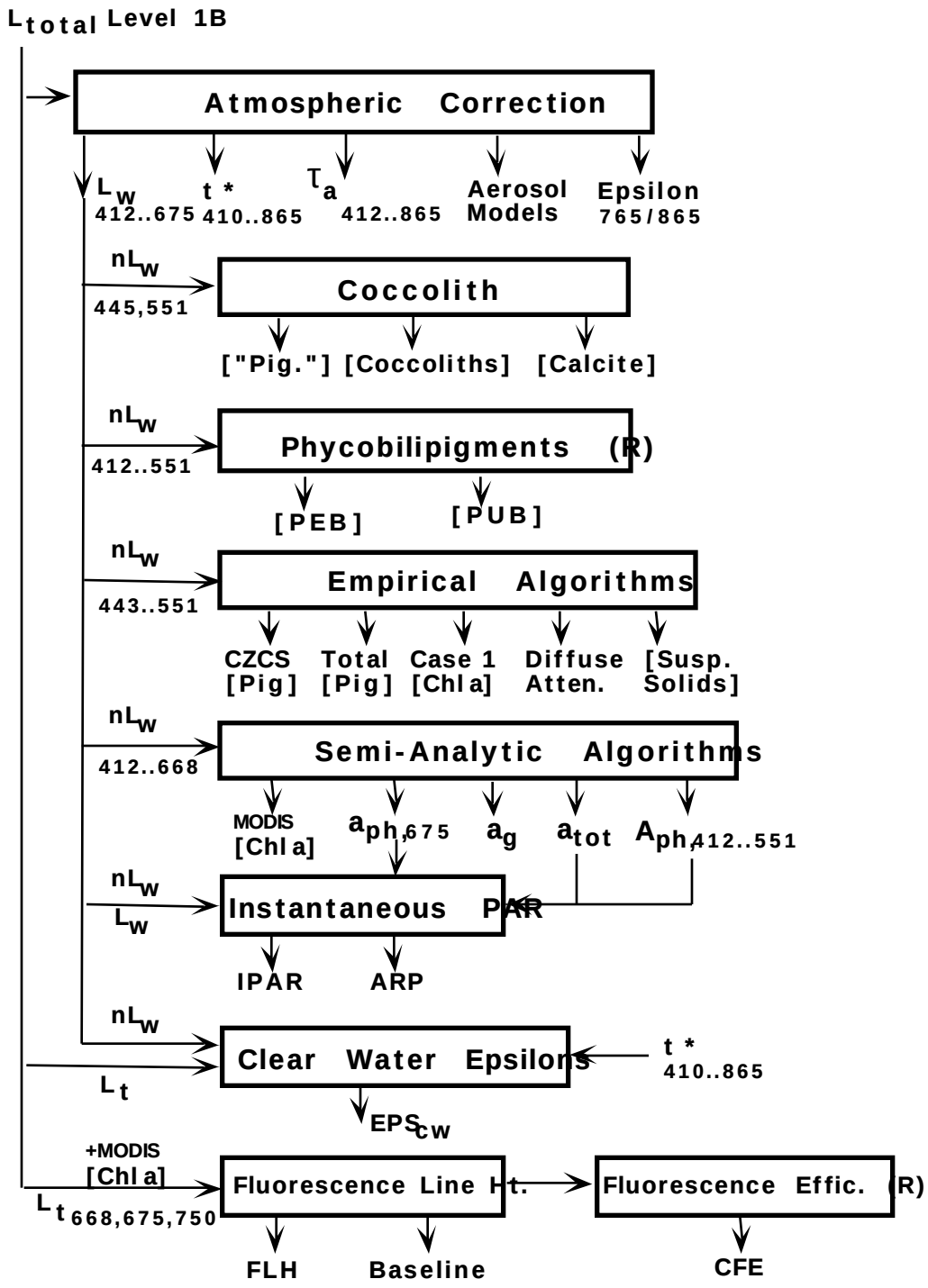

Figure 3. Ocean Bio-optical Data Flow, Level 2 products.

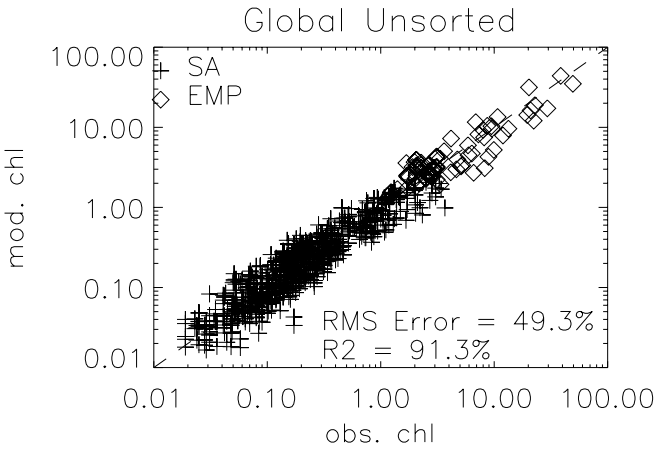
Global Unsorted
SA
EMP
RMS Error = 49.3%
R2 = 91.3%
mod. chl
obs. chl
0.01
0.10
1.00
10.00
100.00

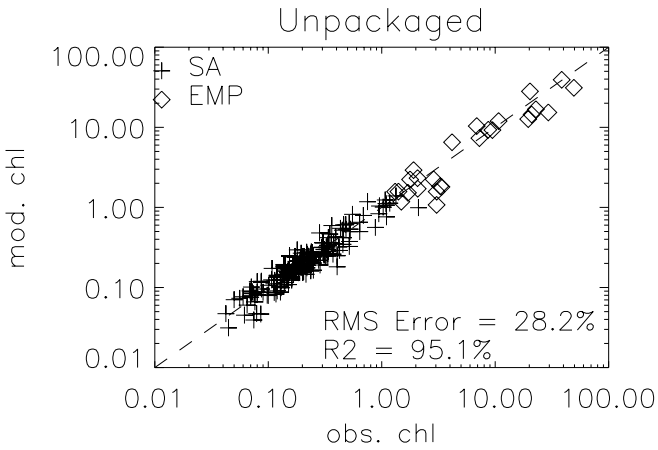
Unpackaged
SA
EMP
RMS Error = 28.2%
R2 = 95.1%
mod. chl
obs. chl
0.01
0.10
1.00
10.00
100.00

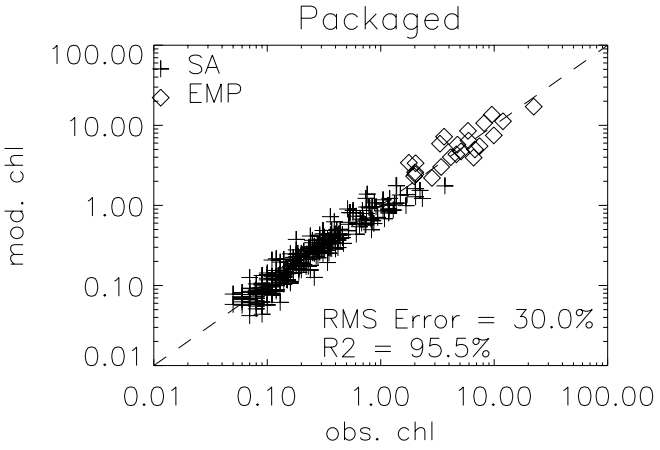
Packaged
SA
EMP
RMS Error = 30.0%
R2 = 95.5%
mod. chl
obs. chl
0.01
0.10
1.00
10.00
100.00

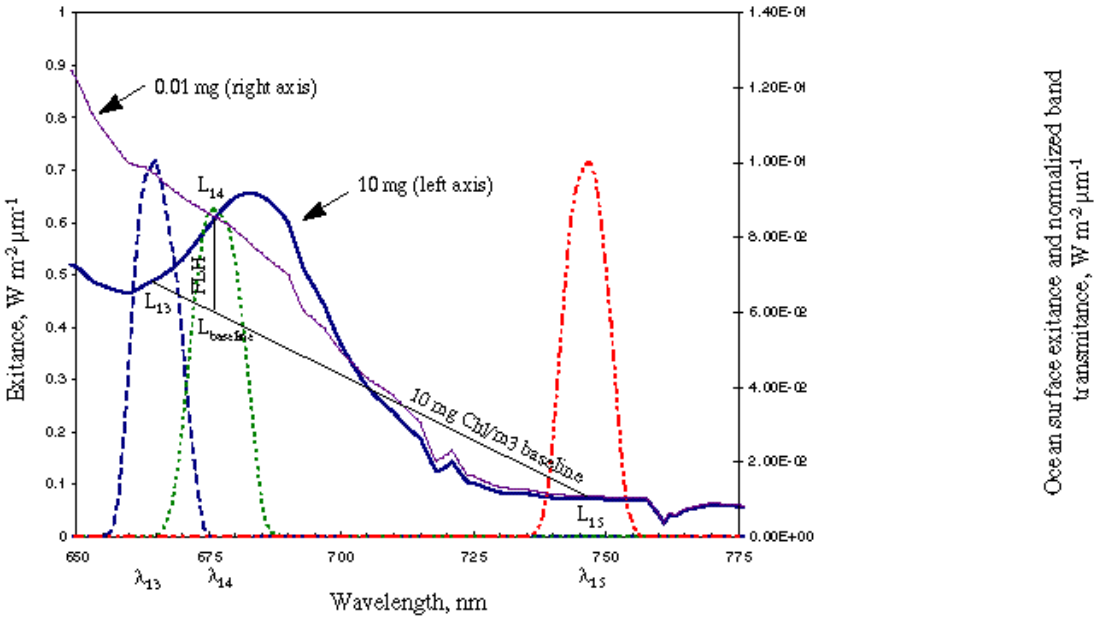
0.01 mg (right axis)
10 mg (left axis)
L14
L13
FLH
Lbaseline
10 mg Chl/m3 baseline
L15
λ13
λ14
λ15
Wavelength, nm
Exitance, W m-2 µm-1
Ocean surface exitance and normalized band transmitance, W m-2 µm-1

Figure 5

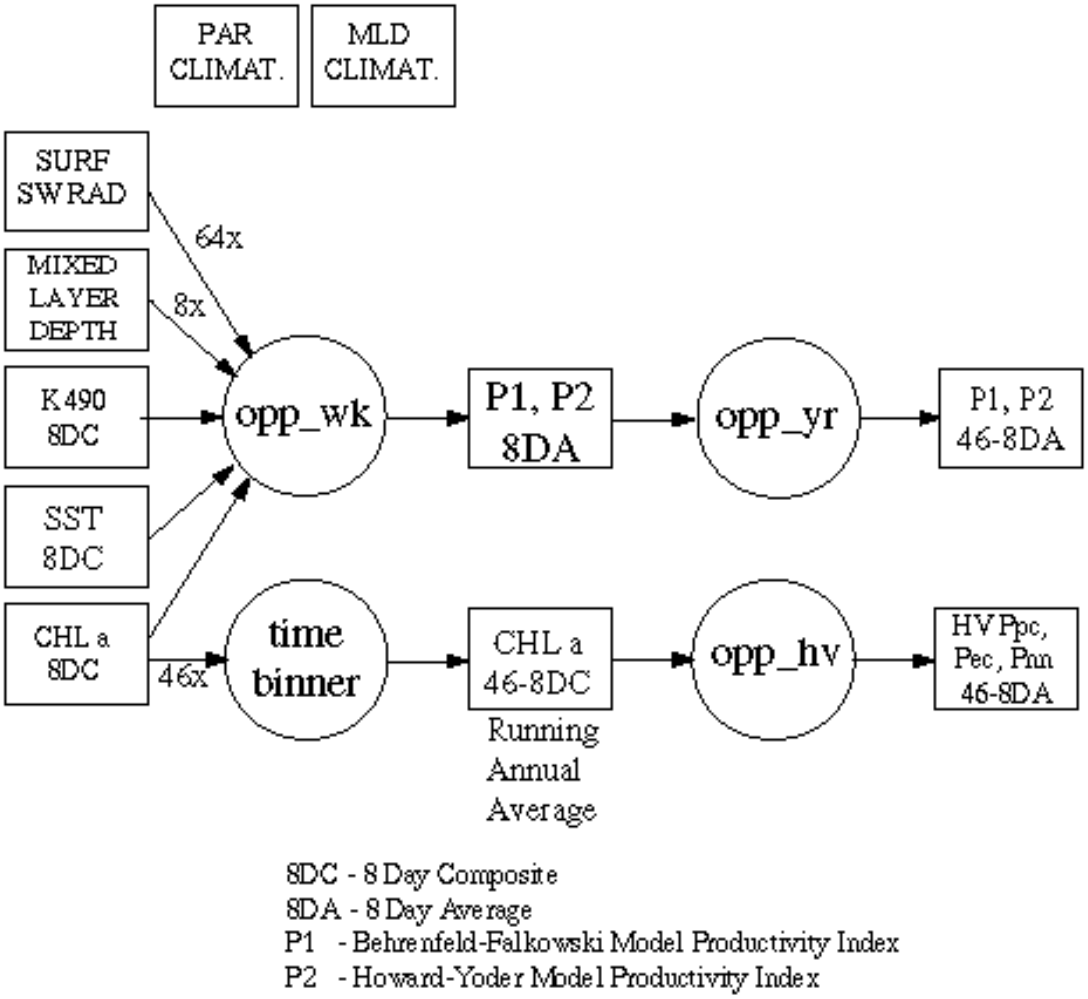
PAR CLIMAT.
MLD CLIMAT.
SURF SWRAD
MIXED LAYER DEPTH
K490 8DC
SST 8DC
CHL a 8DC
64x
8x
46x
opp_wk
time binner
P1, P2 8DA
CHL a 46-8DC
Running Annual Average
opp_yr
opp_hv
P1, P2 46-8DA
HV Ppc, Pec, Pnn 46-8DA
8DC - 8 Day Composite
8DA - 8 Day Average
P1 - Behrenfeld-Falkowski Model Productivity Index
P2 - Howard-Yoder Model Productivity Index

Figure 6.

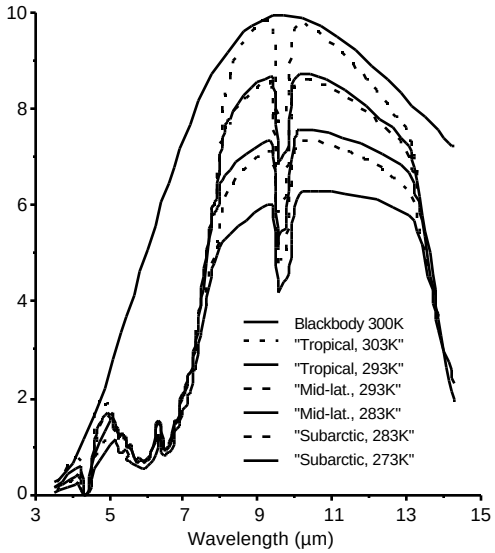

Figure 7. Earth radiance in the mid- to far-infrared spectrum. The various curves give a range of expected infrared radiances for a variety of typical atmospheres and surface temperatures. A 300K blackbody curve is provided to permit visual comparison of the path length absorption for the various cases. Profile data is computed by the Lowtran radiative transfer program [Selby *et al.*, 1978].